How far does the tree affect the crop in agroforestry? New spatial analysis methods in a Faidherbia parkland

Olivier Roupsard, Alain Audebert, Adama Ndour, Cathy Clermont-Dauphin, Yelognissè Agbohessou, Josias Sanou, Jonas Koala, Emile Faye, Diaretou Sambakhe, Christophe Jourdan, et al.

How far does the tree affect the crop in agroforestry? New spatial analysis methods in a *Faidherbia* parkland

Olivier Roupsard[a,b,c*] , Alain Audebert[d,e,f], Adama P. Ndour[f], Cathy Clermont-Dauphin[g,c], Yelognissè Agbohessou[c,h], Josias Sanou[i], Jonas Koala[j], Emile Faye[k,l], Diaretou Sambakhe[f], Christophe Jourdan[a,b,c], Guerric le Maire[m,b], Laure Tall[n,c], Diaminatou Sanogo[h], Josiane Seghieri[b], Laurent Cournac[b], Louise Leroux[o,p,q]

[a]CIRAD, UMR Eco&Sols, Dakar, Senegal
[b]Eco&Sols, Univ Montpellier, CIRAD, INRAE, IRD, Montpellier SupAgro, Montpellier, France
[c]LMI IESOL, Centre IRD-ISRA de Bel Air, Dakar, Senegal
[d]CIRAD, UMR AGAP, Thiès, Senegal
[e]AGAP, Univ Montpellier, CIRAD, INRAE, INRIA, Montpellier SupAgro,
[f]CERAAS, ISRA, Thiès, Sénégal
[g]IRD, UMR Eco&Sols: LMI IESOL, Dakar, Senegal
[h]CNRF, Dakar, Senegal
[i]INERA, DEF, Ouagadougou, Burkina Faso
[j]INERA, DRREA, Centre Saria, Burkina Faso
[k]CIRAD, UPR HortSys, Montpellier, France
[l]CDH, ISRA, Dakar, Senegal
[m]CIRAD, UMR Eco&Sols, Montpellier
[n]LNRPV, ISRA, Dakar, Senegal
[o]CIRAD, UPR AIDA, Dakar, Senegal
[p]AIDA, Univ Montpellier, CIRAD, Montpellier, France
[q]CSE, Dakar, Senegal

*Corresponding author: olivier.roupsard@cirad.fr: O. Roupsard, CIRAD, LMI IESOL, BP 1386, CP 18524, Dakar, Senegal. Tel. (+221)786017233

Abstract

The trees in agroforestry plots create spatial heterogeneity of high interest for adaptation, mitigation, and the provision of ecosystem services. But to what distance, exactly, from the tree? We tested a novel approach, based upon geostatistics and Unmanned Aerial Vehicle (UAV) sensing, to infer the distance at which a single agroforestry tree affects the surrounding under-crop, and to map yield, litter (i.e. stover) and crop-partial Land Equivalent Ratio (LER_{cp}) at the whole-plot level.

In an agro-silvo-pastoral parkland of semi-arid western Africa dominated by the multi-purpose tree *Faidherbia albida*, we harvested the pearl-millet under-crop at the whole-plot scale (*ca.* 1 ha) and also in subplot transects, at three distances from the trunks. We observed that the yield was three times higher below the tree crown (135.6 g m^{-2}) than at a distance of five tree-crown radii from the trunk (47.7 g m^{-2}). Through geostatistical analysis of multi-spectral, centimetric-resolution images obtained from an UAV overflight of the entire plot, we determined that the 'Range' parameter of the semi-variogram (assumed to be the distance of influence of the trees on the Normalized difference vegetation index (NDVI)) was 17 m. We correlated the yield (r^2 = 0.41; RRMSE = 48%) and litter production (r^2 = 0.46; RRMSE = 35%) in subplots with NDVI, and generated yield and litter maps at the whole-plot scale. The measured whole-plot yield (0.73 t ha^{-1}) differed from the one estimated via the UAV mapping by only 20%, thereby validating the overall approach. The litter was estimated similarly at 1.05 tC ha^{-1} yr^{-1} and mapped. Using a geostatistical proxy for the sole crop, LER_{cp} was estimated 1.16, despite the low tree density.

This new method to handle heterogeneity in agroforestry systems is a first application. We also propose strategies for extension to the landscape level.

Keywords: Geostatistics / Unmanned Aerial Vehicle (UAV) / Land Equivalent Ratio (LER) / Spectral indices / distance of influence

1 Introduction

Agroforestry provides attractive alternatives to monoculture, especially when the benefits of association can be quantified and explained convincingly based upon phenomena such as extended resource acquisition, complementarity, and facilitation. Even before modern science provided such explanations, the benefits of agroforestry systems had been clear to traditional societies, which made those systems a prominent and enduring feature of their agriculture, especially in the tropics. Agroforestry was largely abandoned during the green revolution Jain (2010), but is enjoying a strong revival and increased interest, particularly in Africa (Mbow *et al.*, 2014), in the context of climate change, food-security concerns, limits to growth (Meadows and Meadows, 2007), and sustainable-development goals (Griggs *et al.*, 2013). Agroforestry systems are part of the bedrock of sustainable intensification because they are compatible with options such as conservation agriculture, agro-silvo-pastoralism, and precision agriculture (Aune *et al.*, 2017).

To what distance does a tree affect specific crop traits, e.g. biomass, productivity, yield, C sequestration, root distribution, resource acquisition, or hydraulic redistribution? Assessing the distance (radial extent) of influence of trees on the under-crops and adjusting tree density are key to managing agroforestry systems, with direct impacts on the system's productivity, provision of ecosystem services and capacity to mitigate and adapt to climate changes. However, the difficulty and expense of manipulating tree densities (whether in orchards or in long-term scientific trials) discourages efforts. A partial remedy is the modeling of agroforestry *in silico*, which extends our ability to test optional densities under various scenarios (van Noordwijk and Lusiana, 1998; Luedeling *et al.*, 2016; Vezy *et al.*, 2018; Dupraz *et al.*, 2019; Vezy *et al.*, 2020), although within the limits of validation.

A common assumption is that trees must influence the crop anyhow, even at large distances, above or belowground (Luedeling *et al.*, 2016) and that the distance of influence depends on the crop trait of interest. Can we assess that distance for a single crop trait at least, like yield for instance? What is the pattern of influence? Is the effect multinomial, such as for windbreaks for example (McNaughton, 1988) or rather monotonic? Solving the question, trait by trait and statistically would simplify the process of adjusting tree density, according to the local priority. The usual way to address this issue experimentally is by designing subplot arrays in the form of rings or logarithmic spirals (Tomlinson *et al.*, 1998) around the agroforestry trees, or in the form of transects between them (Louppe *et al.*, 1996). Given the large heterogeneity induced by the trees, this requires a huge amount of replicates and field work and it is unlikely that it could be extrapolated at the whole-plot or landscape scale. However, the issue can also be framed as a problem in spatial- or geo-statistics, and investigated using interpolation solutions that treat the phenomena of interest (such as crop traits, or in-soil C stocks) as random variables within the tree interspace. In a recent review, Bayala *et al.* (2015) proposed combining yield mapping with geostatistics to address parkland effects on crops, accounting for directional variability. Surprisingly, there were few geostatistical applications under agroforestry so far: most of them characterize spatial dependence of soil properties (e.g. Simon *et al.* (2013)), fewer on crop traits (e.g. Mora and Beer (2013)) and hardly any or none on crop yield. We argue that given the high spatial heterogeneity of edapho-climatic conditions induced by the trees in agroforestry systems (Charbonnier *et al.*, 2013; Charbonnier *et al.*, 2014), and the large number of microclimate and productivity random variables that could truly be mapped therein, a great deal of valuable information may yet be brought to light through studies that complement classical experimental designs with geostatistical methods.

That same geostatistical information may help agroforestry systems fulfil their potential to provide reasonable options for mitigation, adaptation, and resilience in the face of climate changes (Albrecht and Kandji, 2003; Kumar and Nair, 2011; Lorenz and Lal, 2014; Zomer *et al.*, 2016). In that respect, too, the densities of an agroforestry system's trees and under-crop are important. Regarding mitigation, the build-up of tree perennial biomass stores C rapidly, but in the short term, whereas soil stores C for the long term, but via slow processes of uptake from the litter (crop residues, or stover), and only a small part of this achieves long residence times in stable organic matter pools. Crop productivity, litter, and SOC build-up are key factors in the long term (e.g. throughout rotations). We argue that neither the crop biomass and productivity (and its partitioning between residuals and exports), nor the soil component, nor the spatial variability of C sequestration inside the agroforestry plot should be neglected when estimating mitigation, especially for the long term. Here, again, is where geostatistics may prove valuable. The under-crops and the soil were long neglected or assumed to be neutral for C sequestration in agroforestry systems. They were not even accounted for in the IPCC guidelines (Smith *et al.*, 2014). Only recently did Cardinael *et al.* (2018b) review coefficients for estimating C storage rates in biomass and soil, according to the type of land-use change (LUC) and the world region—an effort to be further incorporated into Tier 1 IPCC guidelines. We argue that any method that could map metrics for crop biomass, C stock, NPP, and litter inside heterogeneous agroforestry systems has the potential to further improve Tier 1 coefficients.

Similar comments—including those regarding the crucial importance of tree density and of the distance to which the trees influence the under-crop— apply to agroforestry systems' capacities for adaptation. It is often assumed that agroforestry trees create 'islands of fertility' around them (Félix *et al.*, 2018). That is, trees may improve the microclimate locally, along with the soil's infiltrability and its physical, chemical, and biological conditions.

Overall, the tree density and distance of influence of the trees on crops appear as a crucial aspect facing climate changes, both for mitigation and adaptation. Climate change could imply afforestation, reforestation and increase in tree density in conditions where the ecosystems were degraded, or where ecological intensification is needed, with consequences for mitigation and adaptation of climate change policies. The trade-offs between ecosystem services carry to scrutiny in the context of a modification of tree density and the question of adoptability is crucial. Any means to demonstrate the benefits on crop productivity and C stock or storage inside heterogeneous agroforestry systems, such as mapping and quantifying finely those variables under a range of tree densities, should be reflected in the impact.

Remote sensing and proxy-detection are attractive tools for the necessary mapping of target crop traits. As one example, the estimation of yields of cereal crops in a complex agricultural landscape was made possible by the democratization of satellite imagery of high spatial-temporal resolution (VHR: e.g. Sentinel-2, Landsat 8 or PlanetScope). Leroux *et al.* (2019) exploited the VHR pathway in their recent study of an agroforestry parkland with an under-crop of millet. They showed how the assessment of agronomic performances at the whole-plot level can be improved by integrating structural information from the parkland with a statistical model for estimating millet yields via remote sensing. However, this type of approach based upon yield subplots chosen randomly in the landscape could not integrate the intra-plot variability: therefore, it could not investigate the effects of environmental micro-variability, or the farmers' precision practices, or the local impact of trees.

In contrast, unmanned aerial vehicles (UAVs) can assess intra-plot variability even in heterogeneous agricultural landscape of smallholder farming system, thereby complementing satellite VHR data (Schut *et al.*, 2018). The potential of UAVs for that purpose remains to be exploited fully. In Padua *et al.* (2017), a review of practical applications of UAVs in agroforestry, and in Adao *et al.* (2017), a forecast of developments in hyperspectral imaging, we found few examples where UAVs were used to study systems with perennials and an under-layer. Rare examples were studied of orchards, considering only the fruit trees therein (Sarron *et al.*, 2018). None considered the under-crop in an agroforestry system. Indeed, we are not aware of any studies that used UAV to obtain fine-scale data that was then analysed by geostatistical methods to address the central question of the distance at which the trees influence the under-crop. Therefore, we propose this novel approach here: we first assess yield and litter (a proxy for C input to the soil) of the under-crop classically, from subplot arrays. Second we scale those variables to the whole-plot level via a method that involves UAV-based mapping of spectral vegetation indices and correlation between spectral indices and groundtruth. Third we compute the distance of influence of the trees according to the geostatistical parameter 'Range'.

Based upon our results, we also propose a new variant of the land-equivalent ratio (LER). LER is a standard index for comparing the performances of crops in association *vs.* sole crops (i.e., those in separate monoculture fields) (Mead and Willey, 1980). The LER is defined as the ratio of the amounts of land that each of those agricultural systems requires in order to give the same production.

For a crop under trees, Mead and Willey (1980) computed the LER as

$$LER = LER_C + LER_T = \frac{Yi_C}{Ys_C} + \frac{Yi_T}{Ys_T}, \qquad \text{(eq. 1)}$$

where the subscripts C and T denote the crop and the tree, respectively; Y_i is the yield in intercropping; and Y_s is the yield in sole-cropping.

A LER greater than 1 indicates that the agroforestry system uses land more productively than sole-cropping. Although equation 1 gives a single LER value for the system, each term on the right-hand side is, in effect, the LER for its respective species. These partial LER are useful when data for only one crop partner is available or of direct interest: for instance it can be calculated for the crop only, if there is no pure tree plot available. However, even when targeting the crop-partial LER (LER_{cp}) only, one is limited when landscape of interest has few treeless areas. Because the few treeless patches that do exist therein may not be representative of (for example) prevailing soil conditions, basing an LER upon crop yields from those patches is risky. The work that we report here may offer a way out of that conundrum. We propose a method, based upon geostatistical inference, for determining the distance beyond which a tree in the agroforestry system of interest does not affect the under-crop, allowing to compute the crop-partial LER (LER_{cp}) directly within complex agroforestry systems.

In summary, the aims of the present study are to: (i) quantify the distance of influence of the tree on the under-crop; (ii) upscale productivity and litter results from small sampling plots to the whole stand through UAV-based mapping of spectral indices; and (iii) propose a simple method to assess LER_{cp} within agroforestry systems where no true sole-crop control is available.

Our study site is a *Faidherbia albida* parkland located in the groundnut basin of Senegal, western Africa, with pearl millet as the under-crop. *Faidherbia albida* is a multipurpose tree. It is emblematic of agroforestry in dry Africa because of its widespread adoption by rural peoples, with generally positive effects upon associated crops (CTFT, 1988). In contrast, pearl-millet (*Pennisetum glaucum*, L.) is the sixth cereal in terms of world production, with crucial role for food security in arid areas of sub-Saharan Africa and India. It is considered a "cereal of last resort" for farmers in especially challenging, arid conditions (Debieu *et al.*, 2017), where other crops would fail. Thus, pearl millet is a bastion of food security in the face of climate changes.

2 Materials and methods

2.1 Study site, soil and climate:

The study was conducted in the agroforestry parkland of Niakhar/Sob, in the groundnut basin of Senegal, western Africa (region of Fatick, 135 km East of Dakar). Within the site is a 50-year-old observatory, the Health and Demographic Surveillance System (HDSS-Niakhar, https://lped.info/wikiObsSN/?HomePage) (Delaunay *et al.*, 2018). The soil is sandy and very poor (0-20 cm layer: >85% sands; <1% clay; CEC < 2%; pH_{H2O} ca. 5.7) and several meters deep. It overlies an Eocene limestone bedrock. A brackish water table is present at around 6 m.

The climate is soudano-sahelian, with a wet season from June to October, followed by an eight-month dry season. According to Lalou *et al.* (2019), rainfall decreased from 900 to 400 mm between 1950 and 1995 (the driest period), then recovered partially to ca. 500 mm by 2015. The seasonal distribution shifted during that recovery period: less rain now falls during the early part of the wet season, and more at the end. The year 2018 was typical of the new distribution: only one heavy rain (*haboob*) fell by the end of June, allowing pearl millet to germinate. The ensuing dry spell, which lasted until August, reduced crop growth and threatened the crop's very survival. The year's total rainfall, as was measured on site with an automatic tipping bucket (Texas Electronics, model TE525mm), was 454 mm.

Early that year, during the dry season, we launched the highly instrumented "Faidherbia-Flux" site (http://agraf.msem.univ-montp2.fr/Senegal.html). It was set up within farmers' active agro-silvo-pastoral bush fields, which are dominated by the multipurpose tree *Faidherbia albida* (Del.) A. Chev. In an area of 15 ha surrounding the experiment, the faidherbia density was 6.8 tree ha^{-1} and the canopy cover was 5.14 %. The under-crop here is a mosaic of crops, including pearl-millet ('Souna', a traditional, 90 days cycle duration, low photoperiodic and heterogenous millet variety), groundnut, watermelon, cowpea, and fallow (Fig. 1). Faidherbia-Flux is located N: 14°29'44.916"; W: 16°27'12.851". It is registered with FLUXNET (http://daac.ornl.gov/FLUXNET/fluxnet.shtml) as 'Sn-Nkr'. To accommodate the research needs of multidisciplinary teams, it has instruments and facilities for monitoring micro-meteorology; eddy-covariance fluxes of sensible heat, latent heat, and CO_2; soil water; temperatures of land surface and soil; NDVI; soil respiration; sapflow; LAI; tree growth; growth of fine roots; crop productivity; and yields. Faidherbia-flux hosts several and multi-disciplinary research teams and is widely open to collaboration

2.2 Production, sampling, and laboratory analyses of the millet under-crop

All of the agricultural practices (e.g. land preparation, sowing, thinning and weeding) were performed by the farmer, according to his usual preferences, habits, and calendar, in order to avoid disrupting long-term dynamic equilibria and ensure that results would be representative. Most management practices were identical whatever the tree presence, with exception to weeding probably, that occurred to be more necessary at large distances from the tree (see Results section). However, this should not affect the relationships between crop traits and vegetation indices which are fundamental for our purpose. The geostatistical model is assumed to take the whole intra-plot variability into account.

Only the subplot harvest was performed by the scientific team. For crop yield, growth and litter (i.e. crop residues, or stover) variables, we tested the factor "Distance to tree" with three levels: below the tree crown, and at distances of 0.5 R, 2.5 R, and 5 R, where R is the radius of the tree crown (Fig. 2). We used N = 4 replicates per distance to tree, for a total of 12 subplots.

We pre-selected the four trees and transects using a recent dry-season Google Earth© image, in order to avoid the subjectivity of subplot selection directly in the field. We distributed the subplots accordingly. The radius of each chosen tree was measured on the image, and later confirmed in the field. The average value of the distance from the tree trunk to the 5R subplots always exceeded 20 m.

We fixed the number of sowing pockets (for whatever live or dead plant) per subplot at about 15 (16.4 ± 1.6). Therefore, the area of each subplot varied somewhat (18.8 ± 6.9 m^2), according to the sowing density used by the farmer. The area per pocket was 1.16 ± 0.5 m^2.

During the second week of October 2018, a team of six scientists was dispatched into the field to collect the subplots. We first collected all the ears (millet spikes) from each subplot, then split the vegetative biomass into leaves, stems, and roots (all roots collected in a 20 cm radius hemisphere below the plant) and measured the fresh weights in the field with scales accurate to within one gram. Only five pockets per plot were sent back to the lab for air drying, oven drying (65°C, 72h), and weighing. From the differences between fresh and dry weights, we calculated water contents for each pocket, from which we then inferred the dry biomasses of the whole subplots. We also measured the specific leaf area (SLA: $m^2\ kg^{-1}$) on samples of fresh leaves, and computed the leaf area and the leaf area index (LAI) per subplot. The aerial part of weeds was likewise collected and weighed. LAI of weeds was estimated from above-ground weed biomass, using (as a default) the SLA measured for millet.

To secure an independent validation for the exercise of scaling-up yield from subplots to whole-plot, we assessed the whole-plot yield as well. For the whole-plot harvest, we relied on the farmer and his family. All ears were harvested the day after we collected our subplots, and then packed into bundles before transport to the village. We counted and weighed every bundle, then applied the ratio of fresh weight of ears to dry weight of grain obtained in the lab on the subplot samples.

The litter (amount of crop and weeds residues left-over in the field after harvest, or stover) was computed as the whole biomass minus the crop ears. It was converted into $gC\ m^{-2}$, assuming a conversion rate of 0.47 (Smith *et al.*, 2014) for illustration applications in the field of climate-change mitigation.

All subsequent measurements are reported per unit ground area.

2.3 UAV sensing and derived proxies for vegetation productivity

UAVs were flown on 8 October 2018—the day before the pearl-millet harvest. Due to their reverse phenology, the faidherbia trees were defoliated at that date. To characterize the land cover of the agroforestry system (Fig. 1), we analysed UAV photogrammetry images according to the method described in Sarron *et al.* (2018). For spectral images, the UAV system was a FeHexaCopterV2 hexaCopter (Flying Eye Ltd., www.flyingeye.fr), with two onboard cameras fixed on a two-axis gimbal to point vertically downward. The first camera was an RGB ILCE-6000 digital camera (Sony Corporation, New York, NY, USA) with a 6000 x 4000 pixel sensor equipped with a 60 mm focal length lens. To minimize the blurring effect and noise in the images, the camera was set on speed priority (1/1250 sec) and auto ISO mode. The second camera was an AIRPHEN multispectral camera (www.hiphen-plant.com, Avignon, France) equipped with an 8 mm focal length lens and acquiring 1280 x 960 pixel images. The AIRPHEN comprises six individual cameras equipped with filters centered on 450, 530, 560, 675, 730 and 850 nm, with a spectral resolution of 10 nm. The flight plan was designed with Kopter tools (http://wiki.mikrokopter.de/fr/MikroKopterTool) to cover the entire area and ensure an 80% frontal and lateral overlap along the track. The UAV was flown at 4.5 m s^{-1} and at 50 m.a.g.l. with both cameras capturing images simultaneously at one-second intervals. With this set up, we obtained a ground sample distance (spatial resolution of the images) of 0.6 and 2.7 cm for the RGB and Airphen Multispectral cameras, respectively. The area below the tree crowns was not covered because the UAVs could not navigate those spaces safely.

As a radiometric-calibration target, we followed the recommendations of Jay *et al.* (2019) in using a 2.5 m² carpet panel placed horizontally on the ground at a distance of 1.5 times the height of the closest plants in order to limit adjacency effects. In addition, as geometric ground control points (GCPs) (Kääb *et al.*, 2014), we placed six red discs of 50 cm diameter at corners of the field. The exact positions of these GCPs were defined with a GNSS-GPS providing an accuracy of 2 cm. Each UAV flight was performed around solar noon and lasted about 15 min., during which solar radiation was assumed to be stable.

An automatic image-processing pipeline was designed to generate radiometrically calibrated and geometrically corrected multiband orthoimages using Agisoft PhotoScan digital photogrametric software (PhotoScan Professional 1.4, Agisoft LLC, Russia). Radiometric calibration included automatic correction of vignetting effects. Real reflectances were computed using a reference target positioned to the ground during UAV flights. This target was previously spectrally characterized in controlled conditions. Geometric correction involved, firstly, multiband co-registration to modify and adjust the images' coordinate system to decrease geometric distortions and make pixels in different pictures coincide with the corresponding map-grid points. The co-registration process was based upon the internal GPS from raw image metadata. Orthorectification was then performed using GCPs to increase the accuracy of the generated orthoimages.

We used RGB orthoimages to segment the pearl millet under-crop and remove the soil and the trees. For that purpose, we converted orthoimages from RGB to HSV color space, then carried out thresholding operations over green crops to create a millet mask. Calibrated reflectances in NIR, Red, and Green bands were extracted based on that mask, then used to derive the Normalized difference vegetation index ((NDVI) Rouse *et al.* (1974), according to the following equation:

$$NDVI = \frac{NIR-Red}{NIR+Red} \qquad \text{(eq.2)}$$

We used mostly the NDVI because it is the most widely used index for monitoring and estimating crop physiology and green biomass. We had six other well-known spectral indices for crop vegetation monitoring at hand, namely CTVI (Corrected Transformed Ratio Vegetation Index), GCVI (Green Chlorophyll Vegetation Index), GNDVI (Green Normalized Difference Vegetation Index), NDRE (Normalized Difference Red Edge Index), TTVI (Thiam's Transformed Vegetation Index) and MSAVI2 (Seconded Modified Soil-Adjusted Vegetation Index). Since they were highly correlated, we decided not to combine them into multiple regressions. However, since MSAVI2 presented slightly better correlation results with e.g. yield and litter than NDVI, we presented its results as well. MSAVI2 is a vegetation index modified for the soil effects (Richardson and Wiegand, 1977; Qi *et al.*, 1994) and it is thus well-designed for crop monitoring in sparsely vegetated areas.

$$MSAVI2 = \frac{(2\times NIR+1-\sqrt{(2*NIR+1)^2-8\times(NIR-RED)}}{2} \qquad \text{(eq.3)}$$

Where MSAVI2 is the index value, NIR and RED are respectively the Near Infrared and Red band reflectance from the UAV sensor.

2.4 Geomatics: chain of processes

For this task, we used QGIS (QGIS_Development_Team, 2019) and R (R_Core_Team, 2017). To allow an intersection of the different geospatial layers used in our methodological framework, all layers were projected under the UTM 28 N /WGS84 coordinated references system. The TIF multi-band UAV ortho-image was converted into a mono-layer NDVI or MSAVI2 TIF raster using the rgdal (Bivand *et al.*, 2014) and raster (Hijmans, 2015) libraries in R.

We created shape files in QGIS for the following: the whole-plot; non-cultivated areas (shelters and tower); the cultivated area; crowns of faidherbia trees; and the periphery of those crowns (a proxy for under-crown conditions). We also created shapefiles for eight of the twelve harvested subplots (i.e., only for those at 2.5R and 5R). No shape files were created for the four subplots at 0.5R (below the crown). Indeed, we observed that the UAV could not sense below faidherbia's crowns, despite the trees' defoliated state. We thus used proxies for the 0.5R subplots, i.e., shape files just in the periphery of the four target-tree crowns, assuming that the yield conditions were representative of the 0.5R subplots (verified in Results section). Next, we computed the position of faidherbia centroids. Given the very high resolution (a few cm^2) of the UAV ortho-image, we aggregated each whole image into a grid of *ca.* 5 m^2 cells for the whole-plot and *ca.* 1 m^2 cells for the subplots. Average NDVI or MSAVI2 ± SD was computed for each cell of the grids, and its coordinates recorded.

A distance matrix was computed between each grid cell and the faidherbia centroids. We used the proximal tree only (k = 1), and also took into account the trees outside the limits of the whole-plot.

We used the resulting file, which combined NDVI or MSAVI2 and distance to the proximal tree, to perform geostatistics at the whole-plot scale. The average NDVI or MSAVI2 and per harvest subplot and tree-periphery file was used to correlate with crop productivity and litter.

2.5 Geostatistics

The distance to tree effect, corresponding to the 'Range' parameter, was analyzed with geostatistics in R, from the table of attributes supplied at the end of the geomatics chain, using the libraries gstat (Pebesma, 2004) and sp (Bivand *et al.*, 2008). We plotted semi-variograms of the grid cells' NDVIs according to the distance to the proximal tree crown centroid (a proxy for the position of the tree trunk), up to a maximum distance of 60 m, and following four azimuths (N, S, E, W). The tree crown radius in the plot covered by UAV was quite homogeneous, 4.67 m +/- 0.88 m (SD) so we used absolute distances to the trunk rather than e.g. distances relative to the crown radius. We used the automap library and the autofitVariogram function to select the best geostatistical model, here 'Ste', which is the Matern model parameterized according to (Stein, 2012).

2.6 *Land Equivalent Ratio (LER_{cp})*

The Land equivalent Ratio (LER) is usually computed following equation 1. In the present case, the LER of interest is the crop-partial LER (LER_{cp}) since we have no information on tree-partial LER (absence of pure tree control in the parkland).

We discarded the option of computing LER_{cp} using the measured (i.e. from plant harvest in 5R subplots) values of sole crop yield (Y_s), due to the low spatial representability of the 5R subplots and to our aim of developing a LER_{cp} method independently from harvest. Instead, we used the estimated yields per zone (from UAV-NDVI flights, combined with geostastistics). The estimated yield was mapped using the correlation from Fig. 7d. We split the map into three distinct zones within the whole-plot: (i) below the tree crown (not sensed by UAV, but we used polygons just around the tree crown instead), (ii) between the edge of the tree crown and the limit of the Range, and (iii) beyond the limit of the Range. To compute Y_s, we used the area beyond the Range. The estimated whole-plot yield, Y_i was thus the sum of the average estimated yield in each zone, weighted per area in each zone. We computed the yield estimated for the pixels below the value of the Range only, as another metrics for Y_i. Finally we compared two LER_{cp} values, depending on both options for Y_i.

2.7 *Statistical analysis*

This task was performed using the R software (R_Core_Team, 2017). One-way ANOVAs were performed when the variables met criteria of (i) variance homogeneity according to the Bartlett test, and (ii) normality of distribution of the residues, according to the Shapiro-Wilk test and Q-Q plot. Otherwise, we performed a Kruskal-Wallis non-parametric test. A Tukey honestly significant difference test was then performed between levels inside each factor.

3 Results

3.1 Millet performance in subplots according to the distance to Faidherbia

In the subplots experiment, millet yield was significantly higher ($p = 0.028$; and by a factor of about three) below the tree crown (0.5R: 136 ± 35 SD g_{grain} m^{-2}) than at the largest distance (5R: 48 ± 33 SD g_{grain} m^{-2}) (Fig. 3a; Tab. 1). The yield at the intermediary distance (2.5 R) was not significantly different than and 0.5R and 5R extremes ($p = 0.13$ and $p = 0.56$, respectively) and will not be discussed further.

The stem biomass and total biomass (above + belowground) of millet was also significantly higher at 0.5 R than at 5R ($p = 0.03$ and $p = 0.04$, respectively), again by a factor of about three (Tab. 1). The biomass of weeds was significantly higher ($p = 0.021$) far from the trees, indicating that they may have introduced significant noise in the NDVI or MSAVI2 signals in this study (Fig. 3b).

The litter (i.e. crop residues, or stover) of millet crop + weeds (expressed in gC m^{-2}) was significantly higher at 0.5R (Tab. 1).

The following variables were not significantly different (at the 0.05 level) between 0.5R and 5R (Tab. 1): the NDVI ($p = 0.09$), the MSAVI2 ($p = 0.07$), the leaf dry mass ($p = 0.1$), the specific leaf area (SLA: $p = 0.83$), the leaf area index (LAI: $p = 0.2$), the root dry mass ($p = 0.14$) and the ratio of root mass to total dry mass ($p = 0.33$).

3.2 Distance of influence of faidherbia on the millet crop

We zoomed on the NDVI ortho-image (Fig. 4a) to show one transect example (Fig. 4b) of NDVI in the pearl-millet (left), according to the distance to a faidherbia tree (right). Greener pixels (high NDVI) predominated close to the faidherbia tree and beneath, whereas white bare soil was abundant at a distance. When the UAVs were flown (October), faidherbia was still defoliated, and high NDVI values can be perceived below the tree crowns. However, the high density of branches prevented us from sampling cell grids directly below tree crowns. This finding suggests that optical sensors mounted on UAVs do not give satisfactory results through tree crowns, even for a defoliated tree. Fig 4c shows one pearl millet pocket. The centimetric resolution allows leaves to be distinguished.

Semi-variograms were performed to contrast NDVI of grid cells in the whole-plot cultivated with pearl-millet, and the distance to the centroid of the proximal faidherbia-tree crown (Fig. 5, 6), up to a maximum distance of 60 m. The best model fit (Fig. 6) was ‘Ste’, displaying a monotonic and asymptotic shape. The ‘Range’, which is assumed here to indicate the statistical distance of influence of the faidherbia tree on the crop NDVI, was 17 m. We found little or no effect of the azimuth on the shape of the semi-variograms (Fig. 5). Therefore, on the further assumption that the system was isotropic, we pooled all grid cells before applying the model fit (Fig. 6). The Range was identical for MSAVI2 (data not shown). This distance of influence (the Range) was substantially less than the distance from the 5R plots to the tree (always > 20 m), suggesting that 5R plots were located in an area little affected by the tree, regarding the NDVI or MSAVI2 at least.

3.3 Upscaling yield and productivity from small subplots to the whole plot

At the whole-plot scale, we harvested 52 bundles, whose fresh mass averaged 23.36 ± 2.96 kg each. In the subplots, we obtained a conversion rate (from fresh mass of ears to dry mass of grain) of 0.52 (Tab. 3). The total harvest was thus 632 kg_{grain}, to which we added the 17.63 kg obtained in the subplots. The effective whole-plot area for crops was 8929 m^2. Thus, the measured (from harvest) whole-plot yield was 0.73 t_{grain} ha^{-1}.

We sought correlations between crop traits, or between one single vegetation productivity index, NDVI or MSAVI2, and some crop traits of interest within the 12 harvested subplots

(Fig. 7; Tab. 2). We found a reasonable positive correlation between millet grain yield and millet LAI (Fig. 7a; $r^2 = 0.63$; RRMSE =33%). The correlation was even better between LAI and the whole-plant biomass (Fig. 7b; $r^2 = 0.80$; RRMSE =23%), suggesting that LAI is a good indicator of the millet productivity. However, we found a weaker correlation between LAI and NDVI, for millet + weeds altogether (Fig. 7c; $r^2 = 0.47$; RRMSE =22%): indeed, the NDVI sensed by the UAV was influenced by both crop and weeds; therefore, we had to group them before correlating. Please recall that because the UAV could not sense the 0.5R plots, we used a proxy NDVI from the surroundings of the tree where the 0.5R plot had been harvested. We compared the yield measured in the 0.5R subplots (1.36 t ha^{-1}) with the one estimated from NDVI around the same trees (1.21 t ha^{-1}) and they were actually similar (Table 3), suggesting that using the surrounding of the trees was a reasonable proxy.

For the most crucial correlation here—that between millet grain yield and spectral index of millet+weeds— MSAVI2 (Fig. 7e) performed only marginally better than NDVI (Fig. 7d), thus we decided to stick to NDVI in order to remain more generic. However, both correlations remained pretty loose (NDVI: Fig. 7d and Table 2, $r^2 = 0.41$, RRMSE = 48%; MSAVI2: Fig. 7e and Table 2, $r^2 = 0.47$, RRMSE = 46%).

We found a better correlation between NDVI and litter (expressed in gC m^{-2}) of the millet + weeds (Fig. 7f and Table 2; $r^2 = 0.46$; RRMSE = 35%).

We used coefficients from Fig. 7d to further convert NDVI values into millet grain yield at the whole-plot scale. In the whole-plot millet yield map that we computed using this relationship (Fig. 8a), it can be seen that yield appeared higher near the trees. A slight distance-decay effect is visible as well. We finally validated the yield map (Fig. 8a) using the whole-plot measured yield. The yield estimated from NDVI was 811 kg_{DM} grain for the plot (Tab. 3). Therefore, the error was 20%, which is considered reasonable, in spite of the rather weak relationship obtained in Fig. 7d.

In Fig. 8b, we propose a crop + weed litter map (expressed in gC m^{-2}) as an example for mitigation applications. The UAV-estimated litter production was 1.05 tC ha^{-1} (Tab. 3).

3.4 Measuring and estimating crop-partial LER without a true sole crop reference

In Tab. 3, we computed the crop-partial LER (LER_{cp}) from Eq. 1. The measured LER_{cp} using the estimated whole-plot yield was 1.1. Using the plot yield in the area below the Range only, LER_{cp} was 1.16, both suggesting that the agroforestry system, even at that low tree density (6.8 tree ha^{-1}) spared more than 10% of land.

4 Discussion

What agroforestry research lacks desperately, in order to move beyond the classical dichotomy between shaded and non-shaded plots (Charbonnier *et al.*, 2014), are maps of random variables inside heterogeneous agroforestry systems, for whatever tree spacing. For instance, the MAESPA 3D model (Duursma and Medlyn, 2012) has been applied in agroforestry and 2D horizontal maps have been proposed recently for the light distribution within the crop (Charbonnier *et al.*, 2013), for the crop's surface temperature (Vezy *et al.*, 2018), for crop photosynthesis, transpiration, and water-use efficiency (Charbonnier, 2013), and for light-use-efficiency (LUE) (Charbonnier *et al.*, 2017). 2D and 3D maps of root distribution have been proposed as well, with the uptake of water and nutrients (van Noordwijk and Lusiana, 1998; Dupraz *et al.*, 2019).

Indeed, the ability to produce intra-plot yield maps and inter-plot LER_{cp} is crucial to fostering agroforestry research. This could aid as well in the management of cropping systems, in particular for precision agriculture (for instance varying the crop density according to the distance to the tree), or in mixed-cropping (distributing the crops responsive and non-responsive to the tree effects in the adequate plot locations). In this article, we combined state-of-the-art proxy-sensing technology with a geostatistical method in an original way, to propose a novel statistical approach for assessing the distance at which trees influence crops.

4.1 Upscaling yield from the subplots to the whole-plot through UAV-NDVI

The weak but statistically significant correlation that we found between NDVI and pearl-millet yield (Fig. 7d; $r^2 = 0.41$; RRMSE = 48%) is below the range of correlation found in studies that used remote sensing to estimate pearl-millet yields in West Africa and the MSAVI2 relationship is only marginally better. For example, Rasmussen (1992) in an early study and Leroux *et al.* (2015) both used low-resolution satellite images and were able to explain more than 90% and 65% of the millet-yield variability in northern Burkina Faso and south-western Niger, respectively. The difference between the strength of their correlations and the strength of our own requires some explanations. The first reason is that our study is based on one single plot, so we focused on the intra-plot variability, which is assumed to be much lower than the inter-plot variability normally observed at the landscape scale, thus affecting the correlation; (ii) we used pure spectral indices only, not mixed with covariates such as microclimate or soil or practices that do co-vary at the landscape scale (indeed, we tried to combine 7 spectral indices that we had at hand but they were so correlated that we abandoned such a pathway); (iii) the millet was a traditional variety, by nature very heterogeneous, and it suffered from a severe drought in July 2018 (representative of the new rainfall period after the big drought 1970-2000, though), with impact on survival, which increased the fraction of visible soil and noise; (iv) we could not fly the UAV below the tree crown and relied on a proxy (the difference between measured yield in 0.5R subplots and estimated yield in the periphery of the crown remained small though, Table 3) ; last, the significantly greater amount of weeds (Tab. 1) in the sole crop (5R) may have compensated for the decline of its crop NDVI.

The weakness of our correlation between NDVI and pearl-millet yield likely affected the scaling-up of yield from subplots to the whole-plot, and therefore the value of LER_{cp} that we obtained. Nevertheless, the match between the measured yield and the yield estimated through UAV-NDVI remained satisfactory, with an error below 20% (Tab. 1). It is probable that compensation effects occur at that scale. We suggest that the method proposed here, although affected by a locally-weak calibration at the subplot-scale, may find interesting developments, provided that the calibration phase is improved.

We stress also that one weakness of the work reported here is that the UAV-NDVI yield predictions are based upon a single UAV image acquisition (at harvest), rather than upon images obtained throughout the cropping season. The latter approach generally gives more-accurate estimates of yield because the processes of plant development and growth are nonlinear (Rasmussen, 1992; Maselli *et al.*, 2000; Leroux *et al.*, 2015).

4.2 A new method to assess the distance of influence of the tree on specific crop traits

The distance to which the tree influences the crop is a key topic when designing agroforestry systems. It is a specific trait of a given agroforestry system that underpins the system's overall performances (e.g. net primary productivity, yield, response to climate changes and LER_{cp}). It has received much attention in the past from researchers, who assessed it through complex field experiments that used subplot arrays around the agroforestry trees: e.g. rings (Louppe et al., 1996), logarithmic spirals (Tomlinson et al., 1998), and transects between trees. However, such experiments are so time-consuming and costly that in practice, the tree density is normally fixed by the farmer according to empirical observations or preferences. Scientific experiments come later, by which time the arrangement of trees is generally fixed. As a result, the classical experiment compares agroforestry plots with sole-crop plots, if by chance any are available nearby (Cannavo et al., 2011; Hergoualc'h et al., 2012; Schnabel et al., 2018). Bayala *et al.* (2015) proposed to combine yield mapping and a geostatistical approach as a more systematic way of assessing the tree effects on crop productivity. We developed that approach in the present study. The positive effect of the *Faidherbia albida* tree on the crop yield was demonstrated here in three ways: by photography (Fig. 2), by subplot transects at three distances to the tree (Fig. 3; Tab. 1), and by spectral indices (e.g. NDVI, MSAVI2) measured on the subplot transects (Tab. 1: significant but only at 10%, though). The distance effect itself was quantified through geostatistics of NDVI at the whole-plot scale (Figs 5, 6): we obtained a Range of 17 m, indicating that crop NDVI (same result for MSAVI2), itself correlated to crop yield, was influenced by the tree up to that distance. Even if 17 m is just the beginning of the plateau observed on Fig. 6, it remains a statistical metrics with strong advantages when compared to the classical approach: it statistically defines an unequivocal metrics. Therefore, it can be argued that beyond that limit, the crop's NDVI is statistically unaffected by the trees, according to the model. We stress that this metrics is valid first for the crop spectral index of interest, second for crop traits well correlated to this spectral index, but not for all crop traits in general. Obviously, the tree could affect some other crop traits at larger distances. However, the better the spectral index is correlated to a crop trait of interest (e.g. yield or litter), the better the Range parameter is representative of a statistically significant limit for the trait, between affected and non-affected areas. That latter condition, applied to yield, by definition constitutes sole-cropping. This assertion is in agreement with a recent review by Sileshi (2016), which evidenced through classical methods that faidherbia does not affect pearl millet at distances greater than 16 m from the tree trunk. More specifically, Sileshi (2016) reported that the response ratio, used as a measure of the effect size, was lower than 1, meaning no influence of trees on the crop at a distance of more than 16 m from the trunk.

Actually, the distance of influence on yield and litter measured here by the geostatistical metric Range could vary, according for instance to: other crop traits of interest but not related to a spectral index (e.g. grain quality); the crop species; the microclimate and soil conditions; the density of the crop; the diameter of the tree-crowns and the agricultural practices (e.g. tree pruning, thinning, root cutting, fertilization)... Basically here, we just proposed a method to measure that Range locally, a gateway to test its variability more widely.

4.3 Added value of a metrics for the distance of influence of the tree on crops

Specifically here, we found that the distance of influence for faidherbia upon millet crop NDVI in a range of spacings between trees was, on average, 17 m. We computed that 9.99 (~10) discs of radius = 17 m fit into one ha, according to a staggered arrangement (a 60° diamond pattern being the pattern with the minimum possible empty space left).We can compute that at 10 trees ha^{-1}, 9.3% of the plot is not benefiting from the tree influence. At the tree density in the surroundings of our experimental plot (6.8 tree ha^{-1}, measured on 15 ha), the non-influenced area represents 38% of the plot.

Above 10 trees ha^{-1}, the area of influence of several trees merges. Do we know already how a crop placed under the influence of several trees will behave? No, actually it might depend on (i) the fit of the geostatistical model (Fig. 6), which was monotonic and asymptotic here with a shape very consistent to what was observed through classical methods (Sileshi, 2016), but merging areas could have complex effects with multinomial shapes, such as those encountered for temperature and evapotranspiration in the leeward portions of windbreaks for instance (McNaughton, 1988); (ii) interactions between trees and livestock: a higher tree density might dilute the beneficial effect of the tree, which in the case of faidherbia in a agro-silvo-pastoral parkland is at least partly a result of manure deposition by the livestock (the more trees, the less manure is likely to be deposited under each).

What the Range informs is that 10 trees per ha would minimize the spaces where the millet crop yield is not supported by the trees. There is still a long way, from proposing a metrics for the distance of influence of trees on specific traits of crops, to adjusting the tree density for a variety of ecosystem services or responses to climate changes. However, the above-described method allows to at least minimizing the spaces of no influence, without taking much risk in merging areas of influence, which is an added value when the effect of the tree on the target crop is positive. Therefore, we argue that we can reasonably estimate the yield of crops up to tree densities corresponding to the maximum compaction of discs with radius = Range. Beyond that density, interactions between areas of influence remain unknown.

In addition, the same Range metrics allows to compute LER_{cp}, which is discussed below to extend the added-value.

4.4 Trade-offs when adjusting tree density

Regarding the various ecosystem services that might be worth targeting during the design of tree spacing, a multi-criteria approach is recommended. Trade-offs between ecosystem services should be considered as well: the faidherbia has a positive effect on millet yield and its density could probably be increased from this simple point of view However, a higher density of faidherbia, which is essentially a phreatophytic species (Roupsard *et al.*, 1999), may lower the level of the water table, thereby affecting partitioning between blue and green waters. This specific trade-off is analogous to that for irrigation, and needs to be quantified: consumption of groundwater may be beneficial to food security in the short term, but harmful to sustainability.

A further consideration is that although faidherbia is the parkland's dominant tree species, it is not the only one, and the spatial distributions of the others may affect resources-use patterns among the different components of parkland (Luedeling *et al.,* 2016). Hence, according to the land-use system, effects of faidherbia on crop yields can be mitigated, as already shown in studies conducted at landscape scale (eg. Hadgu *et al.* (2009)).

A final—and delicate—point to consider is the farmer's receptiveness to changing the current tree density, which is the result of tradition combined with his own preference and labour, modulated by constraints (Sambou *et al.*, 2017). Of interest is to investigate how the distance of influence of trees on crops converges with the design that he actually adopted. The Serer tradition recommends 7 faidherbia trees per plot (of ca. 1 ha each) to fill one family's granary (of ca. 5 m^3 each) (R. Diatte, pers. comm.) which is very consistent to what was measured here (6.8 tree ha^{-1}), or also in Lericollais (1972).

4.5 Computing the crop-partial Land Equivalent Ratio (LER_{cp})

The method proposed here offers the possibility to estimate the crop-partial LER in conditions where no true sole crop is available, basing on a metrics for defining the distance of influence of the trees, which is provided by the geostatistical ‘Range’ parameter.

Using that information, researchers can (potentially) identify multiple areas of unaffected under-crop throughout the landscape, for the variable of interest. This method could dramatically extend the range of locations for which LER_{cp} can be estimated. Application of this method at the landscape scale could provide LER_{cp} data for future model validation as well.

The yield of the crop in the agroforestry system, Y_i (eq. 1) is certainly dependent upon the tree density, d, as is the value computed for LER_{cp}: therefore, it would be worth writing them both $Y_{i,d}$ and $LER_{cp,d}$. As we provide the possibility to compute $LER_{cp,d}$ in a wide range of tree densities, such as usually occurring at the landscape scale, it becomes possible to study the relationship between tree density and LER_{cp}. This approach also gives the yield in absence of tree influence (Y_s). Y_s can be seen as a local reference, to study the effect of other variables that affect yield, other than the presence of trees, and that vary in the landscape (e.g. soil fertility, management, etc.). It is a way of standardizing for the effect of trees in the landscape Model simulations could address $Y_{i,d}$, Y_s and $LER_{cp,d}$ as well.

4.6 Applications for Mitigation

The net carbon balance of an ecosystem, often referred to as net ecosystem productivity (NEP) is actually the difference between net primary productivity (NPP) and heterotrophic respiration (R_h) (Roy *et al.*, 2001). Other GHG gases contributing to CO_2eq were considered out of scope here. Therefore, the task of finding ways to calculate the NPP and R_h more conveniently and accurately is central to mitigation accounting. In heterogeneous systems such as agroforestry, maps of fluxes (e.g. yield, NPP per organ, and litter, i.e. crop residues or stover) should improve the C accounting at the whole-plot scale. Tree NPP is key for short-term mitigation (e.g. one rotation), and assessing tree NPP is rather easy from tree-volume functions. Litter input is a fraction of NPP, which in turn is a relatively small fraction of NPP in woody perennials. In contrast, it is a large fraction of NPP in palms, for example (Navarro *et al.*, 2008; Fan *et al.*, 2015), and up to 100% of NPP in annual crops. Assessment of tree litter remains challenging, especially belowground, but can be approached by determining fine-root lifespan in rhizotrons or by sequential coring (Navarro *et al.*, 2008; Defrenet *et al.*, 2016). For crops, which mostly produce litter or exports, we stress that the UAV method proposed above not only allows mapping of crop yield, but potentially, too, of the partitioning of crop NPP into organs that will be exported (e.g. ears) or left to decompose in the plot (litters of stems, leaves, and below-ground biomass). Here, we used UAV to upscale crop litter from subplot to whole plot, and estimated that 1.05 tC ha^{-1} yr^{-1} was left in the field by millet and weeds. R_h does depend upon litter, but its relative contribution to NEP is affected strongly by the local soil's physical, chemical, and biological properties. R_h is difficult to measure, but can be computed from the difference between soil respiration and soil autotrophic respiration, both easier to measure.

Litter is probably the most important variable in SOC build-up (Cardinael *et al.*, 2018a; Fujisaki *et al.*, 2018), together with soil properties, following eq. 4:

$$\Delta C_{soil} = L_A + L_B - R_{soil} + C_{inputs} - C_{exports} \quad \text{(eq. 4)}$$

Where: ΔC_{soil} is the net soil C balance; L is litter (subscripts a is for above-ground and B is for below-ground); R is respiration; C is carbon (inputs are for instance manure; exports is litter removed post-harvest). All expressed in tC ha^{-1} yr^{-1}.

If ΔC_{soil} can be assessed from soil sampling in e.g. synchronic or diachronic experiments, it can also be inferred from the net balance of its C fluxes, as from eq. 4, where above and below-ground litter play key roles.

In this respect, our work is relevant to the Clean Development Mechanisms (CDM) projects. CDM projects could take crops and soil into account, rather than the trees alone. Our methodology also offers the possibility of developing diachronic approaches, which are considered to be more accurate (Costa Junior et al., 2013). In a recent review, Cardinael *et al.* (2018b) stressed that in agroforestry systems worldwide, the ageing and heterogeneity of a plot affects, strongly, the rates at which SOC and biomass accumulate after LUC. Because those rates depend upon the tree density, the method proposed here to improve the crop contribution throughout the landscape should help improve the estimates needed by the CDM projects.

4.7 Applications for Adaptation

Any method that can map crop productivity on a fine scale within heterogeneous agroforest plots will be capable, inherently, of providing the data needed for studying the links between crop performance, distance to tree (or tree planting pattern), microclimate, and fertility. At the landscape scale, that same capability should be useful in screening for favourable or adverse conditions, and for further investigating their determinants (e.g. soil, fertility, or management). Precision agriculture, taking into account the maps of tree influence to adjust crop density or distribute mixed crop species at the field scale could enhance crop productivity and adaptation. We argue here that fine-scale mapping of complex landscapes can identify conditions conducive to adaptation to climate changes. For instance, analysis of the landscape could provide data for drawing response curves relating productivity or LER_{cp} to tree density. This suggestion assumes that trees create 'islands of fertility' and buffer the adverse environment, thereby improving adaptation and resilience. Moreover, from the interpretation of maps of productivity at the landscape scale, it should be possible to survey the 'good practices' of farmers regarding adaptation, after which those practices would be further disseminated.

4.8 Improving the process

Although we argue that the overall process proposed here is valid, we also propose an improved protocol that would refine it: (i) harvest the georeferenced subplots arrays according to randomly chosen distances from the tree (a freedom offered by the geostatistical approach), not necessarily in transects under a factorial plan; (ii) assess the spectral index of the areas below tree crowns manually, using the same camera as on the UAV; (iii) correlate yield (Y_i and Y_s) and crop-partial LER of locations throughout the landscape using co-variables such as microclimate, soil, and agricultural practices; (iv) combine several spectral indices with co-variables to improve yield prediction. This improved methodology can be used also in combination with classical remote sensing (Schut *et al.*, 2018) to bridge intra-plot and inter-plot scales and provide local calibrations for remote-sensing purposes.

5 Conclusions

The distance of influence of the trees upon the under-crops of agroforestry systems, according to specific target services, is crucial to adjusting the tree density for improving productivity and resilience, and to avoiding or minimizing trade-offs. The methodology we propose here is original and infers that distance from UAV mapping of a spectral index, a geostatistical approach, a field calibration, and a validation of the whole-plot yield map.

Although the method still needs development, especially to (i) sense the yield below the tree crown and (ii) combine several spectral indices with co-variables to improve yield prediction, it already opens new avenues for filling some gaps in agroforestry research. Among those gaps are the distance of influence of the tree (a gateway to adjusting tree density); the estimation of litter (i.e. crop residues, or stover) per ha (a gateway for soil C-sequestration models); the computation of crop-partial LER (LER_{cp}) using a reasonable proxy (found directly within the agroforestry plot) for the sole crop; the downscaling of remote-sensing approaches inside agroforestry plots; and the mapping of crop yields at landscape scale while accounting for tree effects.

We invite a large community to test and further develop this new tool, by mapping and comparing yield, NPP, litter, yield under agroforestry, sole-crop yield and crop-partial LER at the levels of the agroforestry plot and landscape.

6 Acknowledgements

The “Faidherbia-Flux” platform is supported by CIRAD, UMR Eco&Sols, LMI IESOL, ISRA, CERAAS and several on-going projects: EU-LEAP-Agri RAMSES II; USAID SIIL-SIMCO; Agropolis and Total Foundation DSCATT; CGIAR GLDC; EU-DESIRA CASSECS; EC2CO ENCAS. The UAV equipment is supported by the Bill and Melinda Gates Foundation through the “Terra-SGT” Project. We thank the people running the Health and Demographic Surveillance System (HDSS), and especially Laurence Fleury, Valerie Delaunay, and Richard Lalou. Among the native people from Sob and Niakhar, we are extremely indebted to Ablaye Diouf, Ibou Diouf, and Robert Diatte. We also thank all the students who are participating in other experiments nearby: Espoir Gablo, Adama Tounkara, Sidy Sow, Seydou Diatta, Sophie Djiba. We are much indebted to Dr. James Smith (https://mx.linkedin.com/in/james-smith-1b195047) for his thoroughful revision of the English. We appreciated and adopted the very useful contributions of our two anonymous reviewers.

7 References

Adao, T., Hruska, J., Padua, L., Bessa, J., Peres, E., Morais, R., Sousa, J.J., 2017. Hyperspectral Imaging: A Review on UAV-Based Sensors, Data Processing and Applications for Agriculture and Forestry. Remote Sensing 9.

Albrecht, A., Kandji, S.T., 2003. Carbon sequestration in tropical agroforestry systems. Agriculture, Ecosystems & Environment 99, 15-27.

Aune, J.B., Coulibaly, A., Giller, K.E., 2017. Precision farming for increased land and labour productivity in semi-arid West Africa. A review. Agronomy for sustainable development 37, 16.

Bayala, J., Sanou, J., Teklehaimanot, Z., Ouedraogo, S., Kalinganire, A., Coe, R., Van Noordwijk, M., 2015. Advances in knowledge of processes in soil–tree–crop interactions in parkland systems in the West African Sahel: A review. Agriculture, Ecosystems & Environment 205, 25-35.

Bivand, R., Keitt, T., Rowlingson, B., 2014. rgdal: Bindings for the Geospatial Data Abstraction Library. R package version 0.8-16. URL http://CRAN. R-project. org/package= rgdal.

Bivand, R.S., Pebesma, E.J., Gomez-Rubio, V., Pebesma, E.J., 2008. Applied spatial data analysis with R. Springer.

Cannavo, P., Sansoulet, J., Harmand, J.M., Siles, P., Dreyer, E., Vaast, P., 2011. Agroforestry associating coffee and *Inga densiflora* results in complementarity for water uptake and decreases deep drainage in Costa Rica. Agriculture Ecosystems & Environment 140, 1-13.

Cardinael, R., Guenet, B., Chevallier, T., Dupraz, C., Cozzi, T., Chenu, C., 2018a. High organic inputs explain shallow and deep SOC storage in a long-term agroforestry system - combining experimental and modeling approaches. Biogeosciences 15, 297-317.

Cardinael, R., Umulisa, V., Toudert, A., Olivier, A., Bockel, L., Bernoux, M., 2018b. Revisiting IPCC Tier 1 coefficients for soil organic and biomass carbon storage in agroforestry systems. Environmental Research Letters 13.

Charbonnier, F., 2013. Measuring and modelling light, water and carbon budgets and net primary productivity in a coffee-based agroforestry system of Costa Rica. PhD. Ecole doctorale RP2E. Université de Nancy I. 19 dec 2013, p. 54 p. + Appendices.

Charbonnier, F., Le Maire, G., Dreyer, E., Casanoves, F., Christina, M., Dauzat, J., Eitel, J., Vierling, L., Van den Meersche, K., Harmand, J.M., Roupsard, O., 2014. The End of the Sun / Shade dichotomy in AFS: mapping of plant light budgets in multistrata heterogeneous plots. Oral Presentation. World Congress on Agroforestry, Dehli, India, 10-14 February 2014.

Charbonnier, F., le Maire, G., Dreyer, E., Casanoves, F., Christina, M., Dauzat, J., Eitel, J.U.H., Vaast, P., Vierling, L.A., Roupsard, O., 2013. Competition for light in heterogeneous canopies: Application of MAESTRA to a coffee (*Coffea arabica* L.) agroforestry system. Agricultural and Forest Meteorology 181, 152-169.

Charbonnier, F., Roupsard, O., le Maire, G., Guillemot, J., Casanoves, F., Lacointe, A., Vaast, P., Allinne, C., Audebert, L., Cambou, A., Clement-Vidal, A., Defrenet, E., Duursma, R.A., Jarri, L., Jourdan, C., Khac, E., Leandro, P., Medlyn, B.E., Saint-Andre, L., Thaler, P., Van den Meersche, K., Aguilar, A.B., Lehner, P., Dreyer, E., 2017. Increased light-use efficiency sustains net primary productivity of shaded coffee plants in agroforestry system. Plant Cell and Environment 40, 1592-1608.

Costa Junior, C., Corbeels, M., Bernoux, M., Piccolo, M.d.C., Neto, M.S., Feigl, B.J., Cerri, C.E.P., Cerri, C.C., Scopel, E., Lal, R., 2013. Assessing soil carbon storage rates under no-tillage: comparing the synchronic and diachronic approaches. Soil and Tillage Research 134, 207-212.

CTFT, 1988. *Faidherbia albida* (Del.) A. Chev. (Synonyme : *Acacia albida* Del.) : monographie. CIRAD-CTFT, Nogent-sur-Marne, France.

Debieu, M., Kanfany, G., Laplaze, L., 2017. Pearl millet genome: lessons from a tough crop. Trends in plant science 22, 911-913.

Defrenet, E., Roupsard, O., Van den Meersche, K., Charbonnier, F., Pastor Pérez-Molina, J., Khac, E., Prieto, I., Stokes, A., Roumet, C., Rapidel, B., de Melo Virginio Filho, E., Vargas, V.J., Robelo, D., Barquero, A., Jourdan, C., 2016. Root biomass, turnover and net primary productivity of a coffee agroforestry system in Costa Rica: effects of soil depth, shade trees, distance to row and coffee age. Annals of Botany 118, 833-851.

Delaunay, V., Desclaux, A., Sokhna, C. (Eds.), 2018. Niakhar Mémoires et Perspectives. Senegal, L' Harmattan Sénégal. Coédition IRD. 536 pp.

Dupraz, C., Wolz, K.J., Lecomte, I., Talbot, G., Vincent, G., Mulia, R., Bussiere, F., Ozier-Lafontaine, H., Andrianarisoa, S., Jackson, N., Lawson, G., Dones, N., Sinoquet, H., Lusiana, B., Harja, D., Domenicano, S., Reyes, F., Gosme, M., Van Noordwijk, M., 2019. Hi-sAFe: A 3D Agroforestry Model for Integrating Dynamic Tree-Crop Interactions. Sustainability 11.

Duursma, R.A., Medlyn, B.E., 2012. MAESPA: a model to study interactions between water limitation, environmental drivers and vegetation function at tree and stand levels, with an example application to [CO2] × drought interactions. Geosci. Model Dev. 5, 919-940.

Fan, Y., Roupsard, O., Bernoux, M., Le Maire, G., Panferov, O., Kotowska, M.M., Knohl, A., 2015. A sub-canopy structure for simulating oil palm in the Community Land Model (CLM-Palm): phenology, allocation and yield. Geosci. Model Dev. 8, 3785-3800.

Félix, G.F., Diedhiou, I., Le Garff, M., Timmermann, C., Clermont-Dauphin, C., Cournac, L., Groot, J.C.J., Tittonell, P., 2018. Use and management of biodiversity by smallholder farmers in semi-arid West Africa. Global Food Security 18, 76-85.

Fujisaki, K., Chevallier, T., Chapuis-Lardy, L., A., A., Razafimbelo, T., Masse, D., Badiane Ndour, Y., Chotte, J.L., 2018. Soil carbon stock changes in tropical croplands are mainly driven by carbon inputs: A synthesis. Agriculture, Ecosystems and Environment. In Press.

Griggs, D., Stafford-Smith, M., Gaffney, O., Rockström, J., Öhman, M.C., Shyamsundar, P., Steffen, W., Glaser, G., Kanie, N., Noble, I., 2013. Policy: Sustainable development goals for people and planet. Nature 495, 305.

Hadgu, K.M., Kooistra, L., Rossing, W.A., van Bruggen, A.H., 2009. Assessing the effect of *Faidherbia albida* based land use systems on barley yield at field and regional scale in the highlands of Tigray, Northern Ethiopia. Food Security 1, 337-350.

Hergoualc'h, K., Blanchart, E., Skiba, U., Hénault, C., Harmand, J.-M., 2012. Changes in carbon stock and greenhouse gas balance in a coffee (*Coffea arabica*) monoculture versus an agroforestry system with Inga densiflora, in Costa Rica. Agriculture, Ecosystems & Environment 148, 102-110.

Hijmans, R.J., 2015. Geographic Data Analysis and Modeling [R package raster version 2.9-5].

Jain, H.K., 2010. Green revolution: history, impact and future. Studium Press LLC, Houston USA.

Jay, S., Baret, F., Dutartre, D., Malatesta, G., Héno, S., Comar, A., Weiss, M., Maupas, F., 2019. Exploiting the centimeter resolution of UAV multispectral imagery to improve remote-sensing estimates of canopy structure and biochemistry in sugar beet crops. Remote Sensing of Environment 231, 110898.

Kääb, A., Girod, L.M.R., Berthling, I.T., 2014. Surface kinematics of periglacial sorted circles using structure-from-motion technology. The Cryosphere 8, 1041-1056.

Kumar, B.M., Nair, P.R., 2011. Carbon sequestration potential of agroforestry systems: opportunities and challenges. Springer Science & Business Media.
Lalou, R., Sultan, B., Muller, B., Ndonky, A., 2019. Does climate opportunity facilitate smallholder farmers' adaptive capacity in the Sahel? Palgrave Communications 5, 81.
Lericollais, A., 1972. Sob: étude géographique d'un terroir sérèr (Sénégal). IRD Editions. 110 p. + Appendices.
Leroux, L., Baron, C., Zoungrana, B., Traoré, S.B., Seen, D.L., Bégué, A., 2015. Crop monitoring using vegetation and thermal indices for yield estimates: case study of a rainfed cereal in semi-arid West Africa. IEEE Journal of selected topics in applied earth observations and remote sensing 9, 347-362.
Leroux, L., Gbodjo, J.E., Djiba, S., Tounkara, A., Ndao, B., Diouf, A.A., Soti, V., Affholder, F., Tall, L., Clermont-Dauphin, C., 2019. Integrating isolated trees improves the agricultural performance assessment of smallholer farming systems at landscape scale in the Senegalese Peanut Basin. 6th Symposium Farming Systems Design. Montevideo, Uruguay.
Lorenz, K., Lal, R., 2014. Soil organic carbon sequestration in agroforestry systems. A review. Agronomy for Sustainable Development 34, 443-454.
Louppe, D., N'Dour, B., Samba, A., 1996. Influence de# Faidherbia albida# sur l'arachide et le mil au Sénégal. Méthodologie de mesure et estimations des effets d'arbres émondés avec ou sans parcage d'animaux.
Luedeling, E., Smethurst, P.J., Baudron, F., Bayala, J., Huth, N.I., van Noordwijk, K., Ong, C.K., Mulia, R., Lusiana, B., Muthuri, C., Sinclair, F.L., 2016. Field-scale modeling of tree-crop interactions: Challenges and development needs. Agricultural Systems 142, 51-69.
Maselli, F., Romanelli, S., Bottai, L., Maracchi, G., 2000. Processing of GAC NDVI data for yield forecasting in the Sahelian region. International Journal of Remote Sensing 21, 3509-3523.
Mbow, C., Van Noordwijk, M., Luedeling, E., Neufeldt, H., Minang, P.A., Kowero, G., 2014. Agroforestry solutions to address food security and climate change challenges in Africa. Current Opinion in Environmental Sustainability 6, 61-67.
McNaughton, K., 1988. 1. Effects of windbreaks on turbulent transport and microclimate. Agriculture, Ecosystems & Environment 22, 17-39.
Mead, R., Willey, R.W., 1980. The Concept of a 'Land Equivalent Ratio' and Advantages in Yields from Intercropping. Experimental Agriculture 16, 217-228.
Meadows, D.H., Meadows, D.L., 2007. The history and conclusions of The Limits to Growth. System Dynamics Review 23, 191-197.
Mora, A., Beer, J., 2013. Geostatistical modeling of the spatial variability of coffee fine roots under Erythrina shade trees and contrasting soil management. Agroforestry Systems 87, 365-376.
Navarro, M.N.V., Jourdan, C., Sileye, T., Braconnier, S., Mialet-Serra, I., Saint-Andre, L., Dauzat, J., Nouvellon, Y., Epron, D., Bonnefond, J.M., Berbigier, P., Rouziere, A., Bouillet, J.P., Roupsard, O., 2008. Fruit development, not GPP, drives seasonal variation in NPP in a tropical palm plantation. Tree Physiology 28, 1661-1674.
Padua, L., Vanko, J., Hruska, J., Adao, T., Sousa, J.J., Peres, E., Morais, R., 2017. UAS, sensors, and data processing in agroforestry: a review towards practical applications. International Journal of Remote Sensing 38, 2349-2391.
Pebesma, E.J., 2004. Multivariable geostatistics in S: the gstat package. Computers & Geosciences 30, 683-691.

QGIS_Development_Team, 2019. QGIS Geographic Information System. Open Source Geospatial Foundation Project. http://qgis.osgeo.org.
Qi, J., Kerr, Y., Chehbouni, A., 1994. External factor consideration in vegetation index development. Proc. of Physical Measurements and Signatures in Remote Sensing, ISPRS 723, 730.
R_Core_Team, 2017. R: A language and environment for statistical computing. R Foundation for Statistical Computing, Vienna, Austria. URL https://www.R-project.org/.
Rasmussen, M.S., 1992. Assessment of millet yields and production in northern Burkina Faso using integrated NDVI from the AVHRR. International Journal of Remote Sensing 13, 3431-3442.
Richardson, A.J., Wiegand, C., 1977. Distinguishing vegetation from soil background information. Photogrammetric engineering and remote sensing 43, 1541-1552.
Roupsard, O., Ferhi, A., Granier, A., Pallo, F., Depommier, D., Mallet, B., Joly, H.I., Dreyer, E., 1999. Reverse phenology and dry-season water uptake by *Faidherbia albida* (Del.) A. Chev. in an agroforestry parkland of Sudanese west Africa. Functional Ecology 13, 460-472.
Rouse, J.W., Haas, R., Schell, J., Deering, D., 1974. Monitoring vegetation systems in the Great Plains with ERTS.
Roy, J., Saugier, B., Mooney, H.A., 2001. Terrestrial global productivity. Academic Press, San Diego. 573 pp.
Sambou, A., Sambou, B., Ræbild, A., 2017. Farmers' contributions to the conservation of tree diversity in the Groundnut Basin, Senegal. Journal of forestry research 28, 1083-1096.
Sarron, J., Malezieux, E., Sane, C.A.B., Faye, E., 2018. Mango yield mapping at the orchard scale based on tree structure and land cover assessed by UAV. Remote Sensing 10.
Schnabel, F., Virginio, E.D., Xu, S., Fisk, I.D., Roupsard, O., Haggar, J., 2018. Shade trees: a determinant to the relative success of organic versus conventional coffee production. Agroforestry Systems 92, 1535-1549.
Schut, A.G., Traore, P.C.S., Blaes, X., Rolf, A., 2018. Assessing yield and fertilizer response in heterogeneous smallholder fields with UAVs and satellites. Field crops research 221, 98-107.
Sileshi, G.W., 2016. The magnitude and spatial extent of influence of *Faidherbia albida* trees on soil properties and primary productivity in drylands. Journal of Arid Environments 132, 1-14.
Simon, N., Montes, F., Diaz-Pines, E., Benavides, R., Roig, S., Rubio, A., 2013. Spatial distribution of the soil organic carbon pool in a Holm oak dehesa in Spain. Plant and Soil 366, 537-549.
Smith, P., Bustamante, M., Ahammad, H., Clark, H., Dong, H., Elsiddig, E.A., Haberl, H., Harper, R., House, J., Jafari, M., 2014. Agriculture, forestry and other land use (AFOLU). Climate change 2014: mitigation of climate change. Contribution of Working Group III to the Fifth Assessment Report of the Intergovernmental Panel on Climate Change. Cambridge University Press.
Stein, M.L., 2012. Interpolation of spatial data: some theory for kriging. Springer Science & Business Media.
Tomlinson, H., Traore, A., Teklehaimanot, Z., 1998. An investigation of the root distribution of *Parkia biglobosa* in Burkina Faso, West Africa, using a logarithmic spiral trench. Forest ecology and management 107, 173-182.
van Noordwijk, M., Lusiana, B., 1998. WaNuLCAS, a model of water, nutrient and light capture in agroforestry systems. Agroforestry Systems 43, 217-242.

Vezy, R., Christina, M., Roupsard, O., Nouvellon, Y., Duursma, R., Medlyn, B., Soma, M., Charbonnier, F., Blitz-Frayret, C., Stape, J.L., Laclau, J.P., Virginio, E.D., Bonnefond, J.M., Rapidel, B., Do, F.C., Rocheteau, A., Picart, D., Borgonovo, C., Loustau, D., Le Maire, G., 2018. Measuring and modelling energy partitioning in canopies of varying complexity using MAESPA model. Agricultural and Forest Meteorology 253, 203-217.

Vezy, R., le Maire, G., Christina, M., Georgiou, S., Imbach, P., Hidalgo, H.G., Alfaro, E.J., Blitz-Frayret, C., Charbonnier, F., Lehner, P., Loustau, D., Roupsard, O., 2020. DynACof: A process-based model to study growth, yield and ecosystem services of coffee agroforestry systems. Environmental Modelling & Software 124, 104609.

Zomer, R.J., Neufeldt, H., Xu, J., Ahrends, A., Bossio, D., Trabucco, A., Van Noordwijk, M., Wang, M., 2016. Global Tree Cover and Biomass Carbon on Agricultural Land: The contribution of agroforestry to global and national carbon budgets. Scientific reports 6, 29987.

[NB: Figures can be printed in colour on the web and in gray scale on paper]

Figure Captions:

Figure 1 Study site, land cover, and experimental display. a/UAV-based map (September 2018, wet season) of "Faidherbia-Flux", located in farmers' agro-silvo-pastoral bush fields, dominated by the multipurpose tree *Faidherbia albida*, here defoliated (white crowns); b/ land-cover map, a mosaic of under-crops (e.g. pearl millet, groundnut, cowpea, watermelon, and grass fallow); c/Overview of the landscape from the eddy-covariance tower (30 m high) during the wet season. The *Faidherbia albida* trees are defoliated, underneath.

Figure 2: Millet-crop sampling at three distances from the *Faidherbia albida* trees. We compared three distances to tree: below the tree crown (0.5 R), at 2.5 radii (2.5 R), and at 5 radii (5R), where R is the radius of the tree crown. N = 4 replicates (4 transects) per distance to tree. Total number of subplots = 12. Note that the development of the millet crop appears to be better below the tree crowns. Image taken from the eddy-covariance tower (September 2018).

Figure 3: Effect of the distance from the faidherbia tree upon two crop traits, as assessed in 12 harvest subplots: a/ pearl-millet yield; b/aerial biomass of weeds. Distances are: below the tree crown (0.5 R), at 2.5 radii (2.5 R) and at 5 radii (5R), where R is the radius of the tree crown. N = 4 replicates (4 transects) per distance to tree.

Figure 4: NDVI sensed by UAV above the agroforestry plot, just before pearl-millet harvest, in October 2018. The greener the color, the higher the NDVI. Faidherbia trees were defoliated, and appear as white discs in the landscape. Bare soil appears white, as well: a/: general overview of the central whole-plot, cultivated in pearl-millet and surrounded by other crops; b/ example of NDVI transect between pearl-millet (left) and a faidherbia tree (right); c/ detail of one pearl-millet plant showing the centimetric resolution of the UAV image.

Figure 5: Directional (N,S,E,W) semi-variograms between NDVI of grid cells in the area of the whole-plot that is cultivated with pearl-millet, and the distance to the centroid of the proximal faidherbia tree crown. The semi-variograms are very similar when using MSAVI2.

Figure 6: Distance of influence of the *faidherbia* tree upon NDVI of pearl millet. Semi-variogram between NDVI of all grid cells in the area of the whole-plot that is cultivated with pearl-millet, and the distance to the centroid of the proximal faidherbia tree crown. The 'Range', or distance of influence is 17 m, corresponding to the red dotted line. The semi-variogram is very similar when using MSAVI2.

Figure 7: Correlations between a single reflectance index (NDVI or MSAVI2) and some crop traits within the harvested subplots (N=12). Because the UAV could not sense the 0.5R plots, we used pixels from the surroundings of the tree where the 0.5R plot had been harvested, as proxy to compute NDVI or MSAVI2,.

Figure 8: Whole-plot maps. a/ yield mapping (orange area) using the relationship from Fig. 7e (scale is in g_{grain} m^{-2}; RMSE = 41.45; RRMSE = 48%); b/map of litter from crop+weeds (scale in gC m^{-2}; RMSE = 48.65; RRMSE = 35%) using the relationship from Fig. 7f. The grey shapes correspond to the faidherbia trees. The grey rectangles are shelters. It can be seen that yield and litter are higher in the surroundings of the trees.

Figure 9

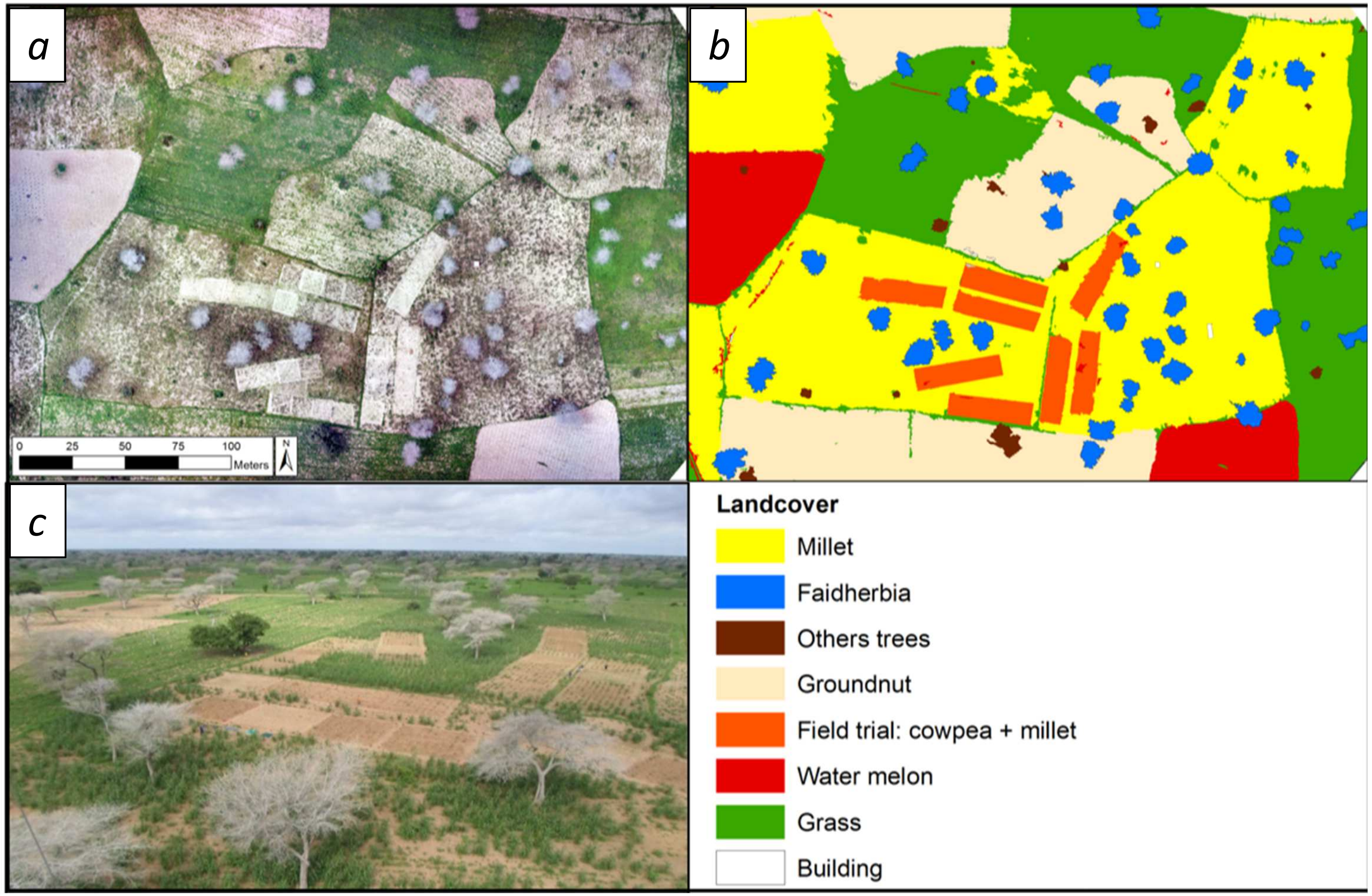
a
b
c
0 25 50 75 100
Meters
N
Landcover
Millet
Faidherbia
Others trees
Groundnut
Field trial: cowpea + millet
Water melon
Grass
Building

Figure 10:

.

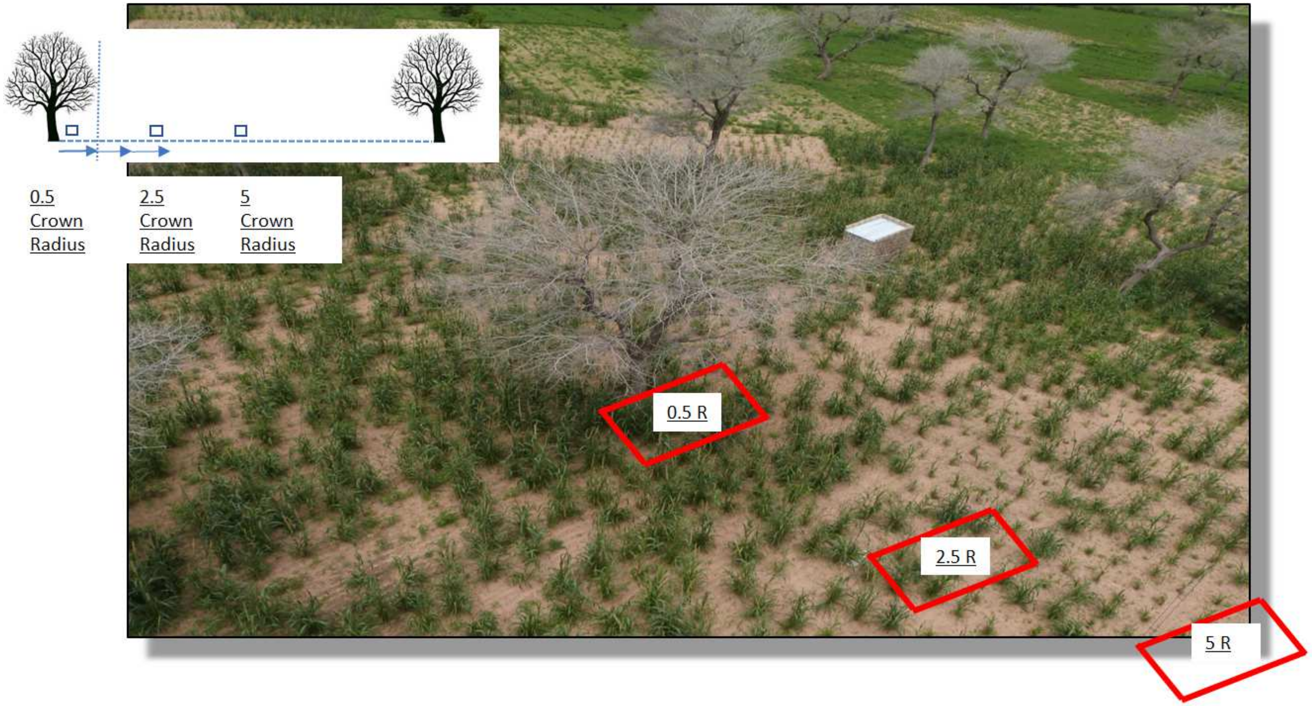

Figure 11:

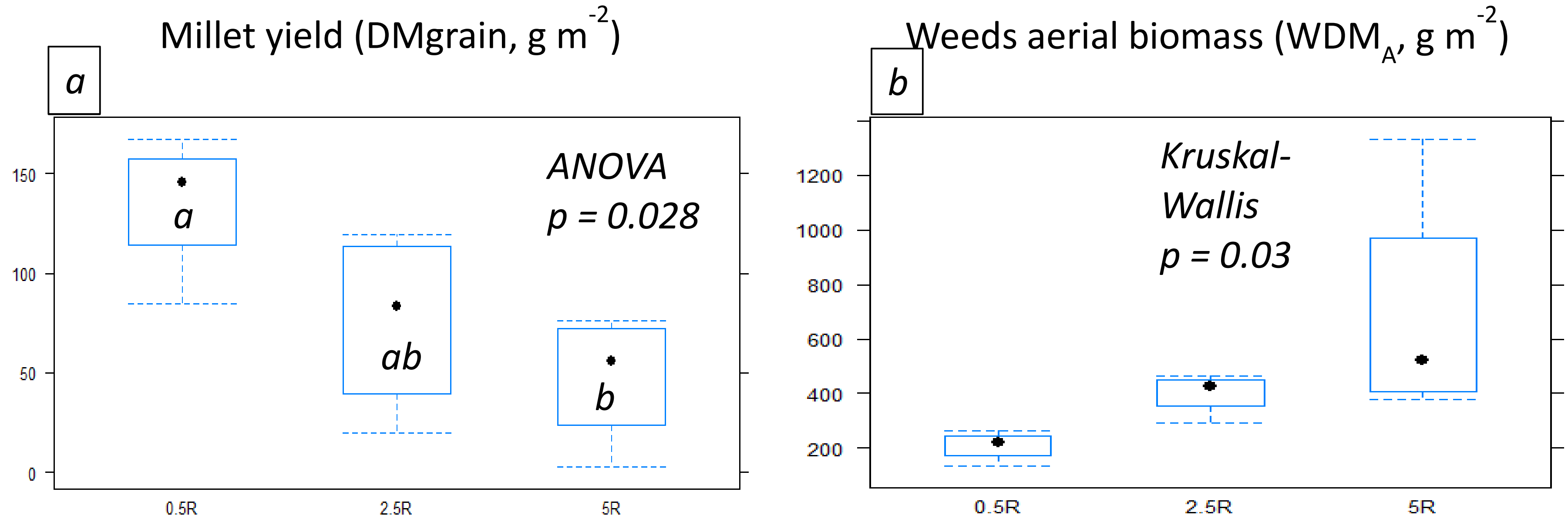

Millet yield (DMgrain, g m-2)
a
150
100
50
0
a
ab
b
ANOVA
p = 0.028
0.5R
2.5R
5R
Weeds aerial biomass (WDMA, g m-2)
b
1200
1000
800
600
400
200
Kruskal-
Wallis
p = 0.03
0.5R
2.5R
5R

Figure 12:

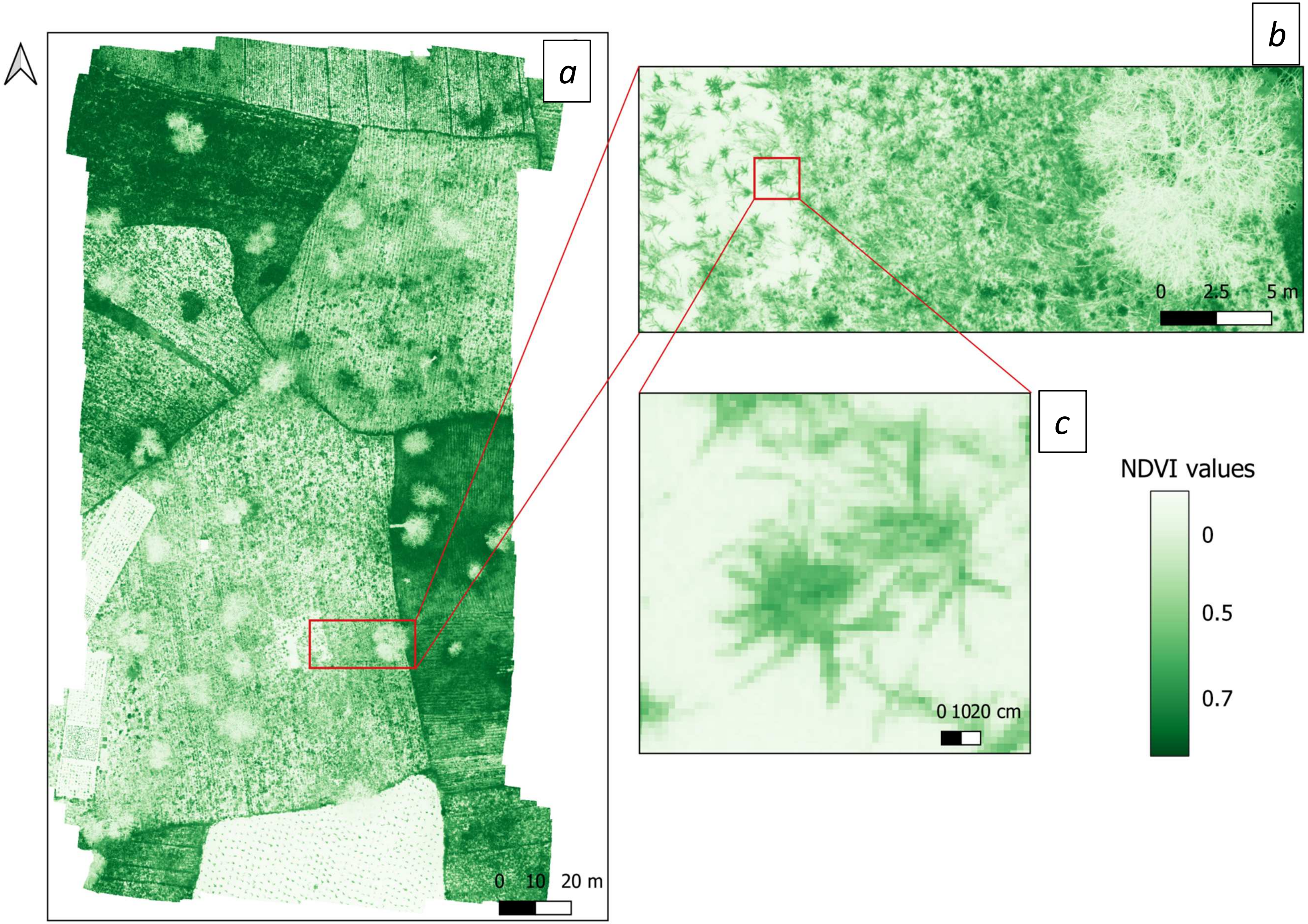

Figure 13:

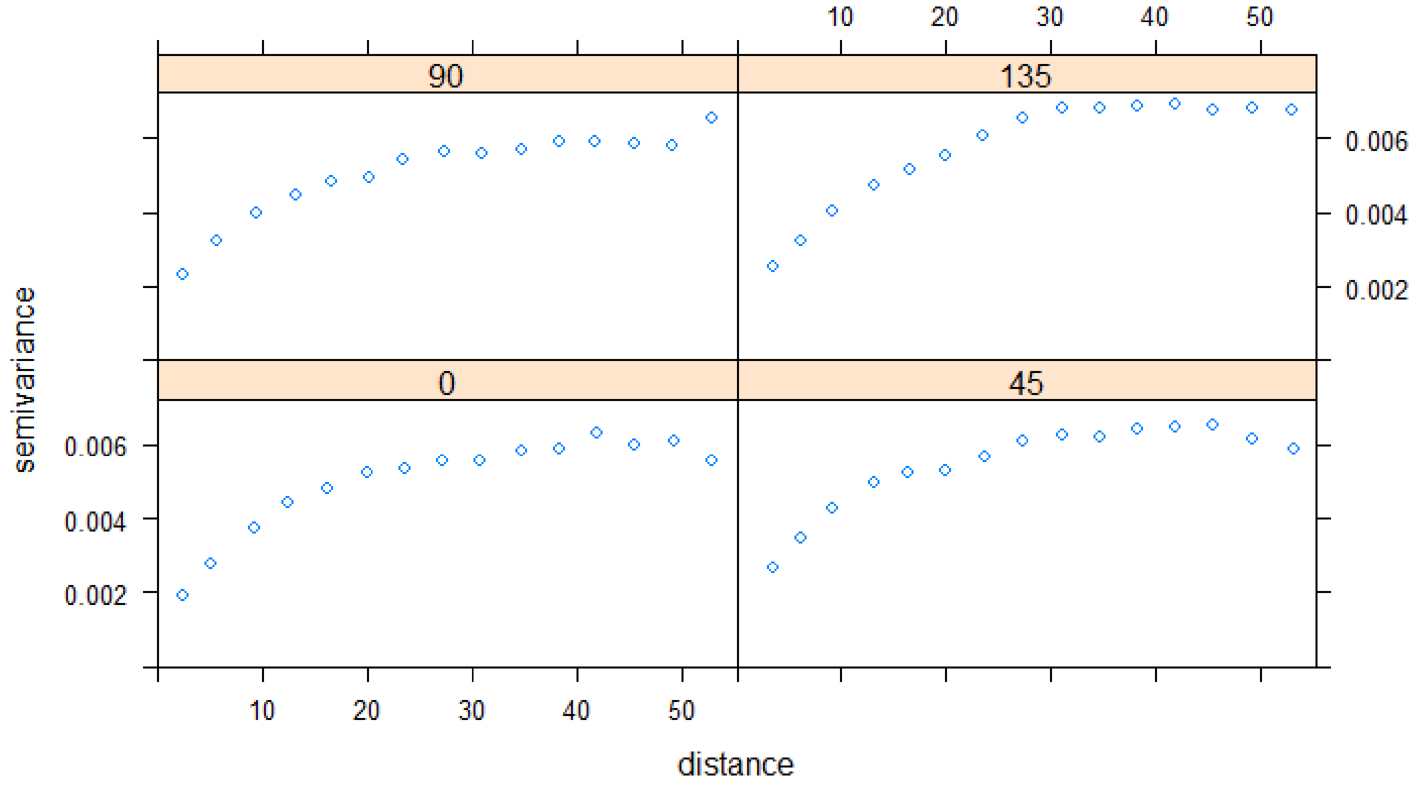
90
135
0
45
semivariance
distance
0.002
0.004
0.006
10
20
30
40
50

Figure 14:

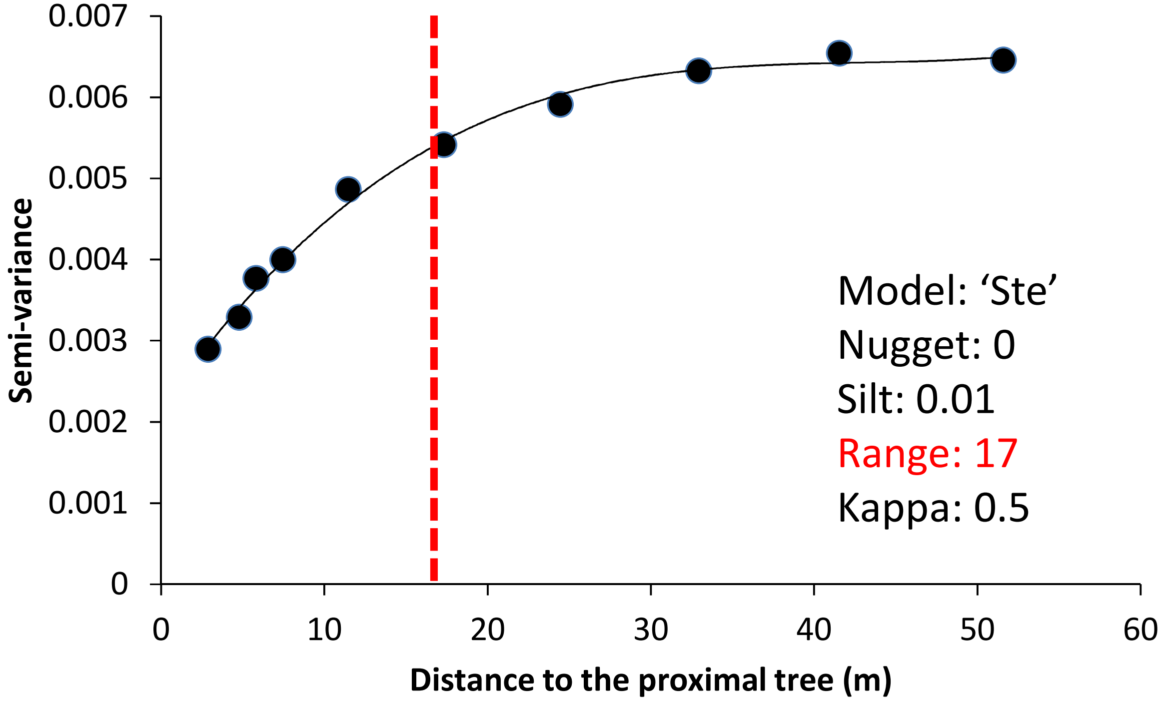

0.007
0.006
0.005
0.004
0.003
0.002
0.001
0
Semi-variance
0
10
20
30
40
50
60
Distance to the proximal tree (m)
Model: 'Ste'
Nugget: 0
Silt: 0.01
Range: 17
Kappa: 0.5

Figure 15:

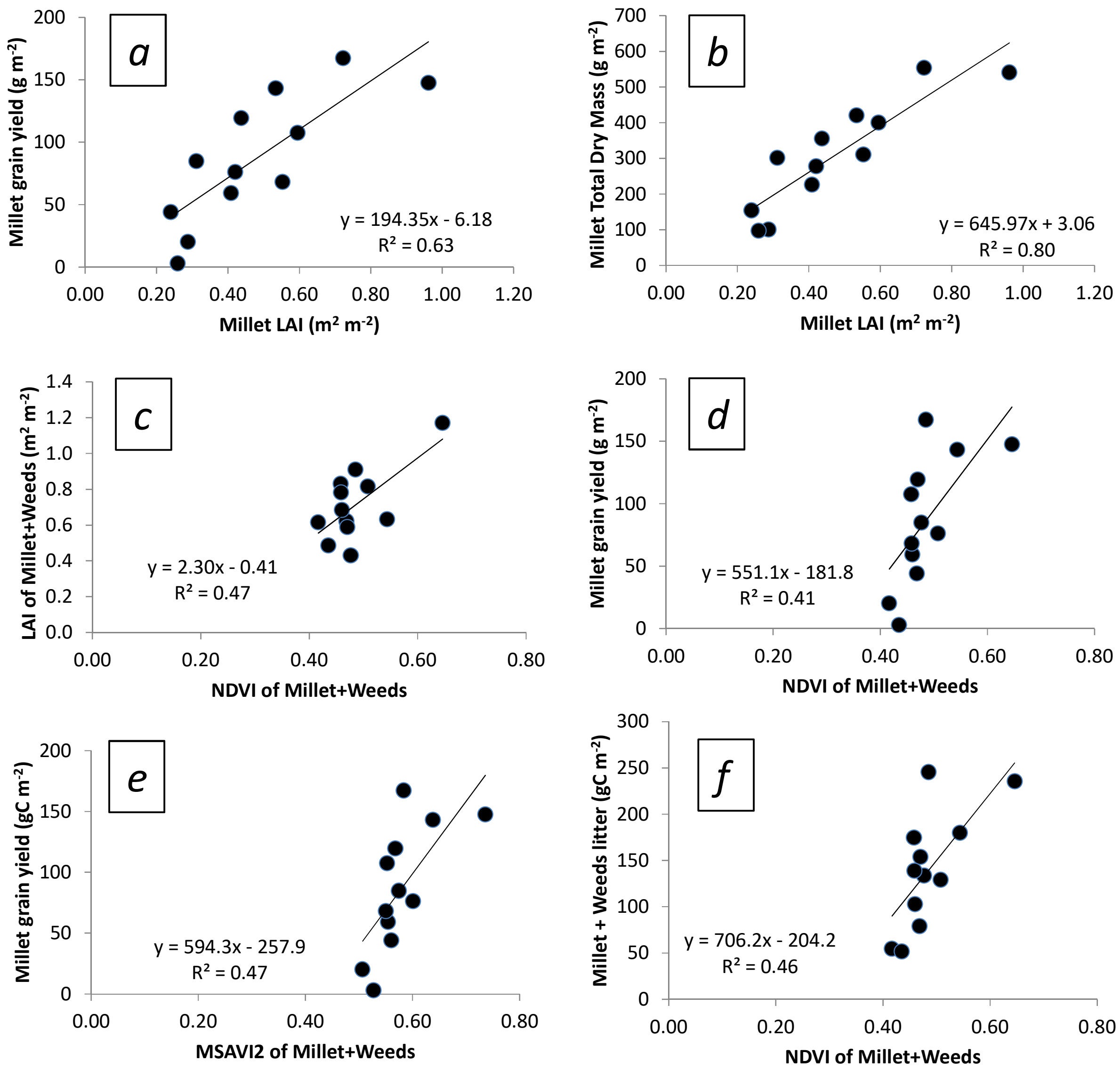
a
Millet grain yield (g m-2)
Millet LAI (m2 m-2)
y = 194.35x - 6.18
R² = 0.63
b
Millet Total Dry Mass (g m-2)
Millet LAI (m2 m-2)
y = 645.97x + 3.06
R² = 0.80
c
LAI of Millet+Weeds (m2 m-2)
NDVI of Millet+Weeds
y = 2.30x - 0.41
R² = 0.47
d
Millet grain yield (g m-2)
NDVI of Millet+Weeds
y = 551.1x - 181.8
R² = 0.41
e
Millet grain yield (gC m-2)
MSAVI2 of Millet+Weeds
y = 594.3x - 257.9
R² = 0.47
f
Millet + Weeds litter (gC m-2)
NDVI of Millet+Weeds
y = 706.2x - 204.2
R² = 0.46

Figure 16:

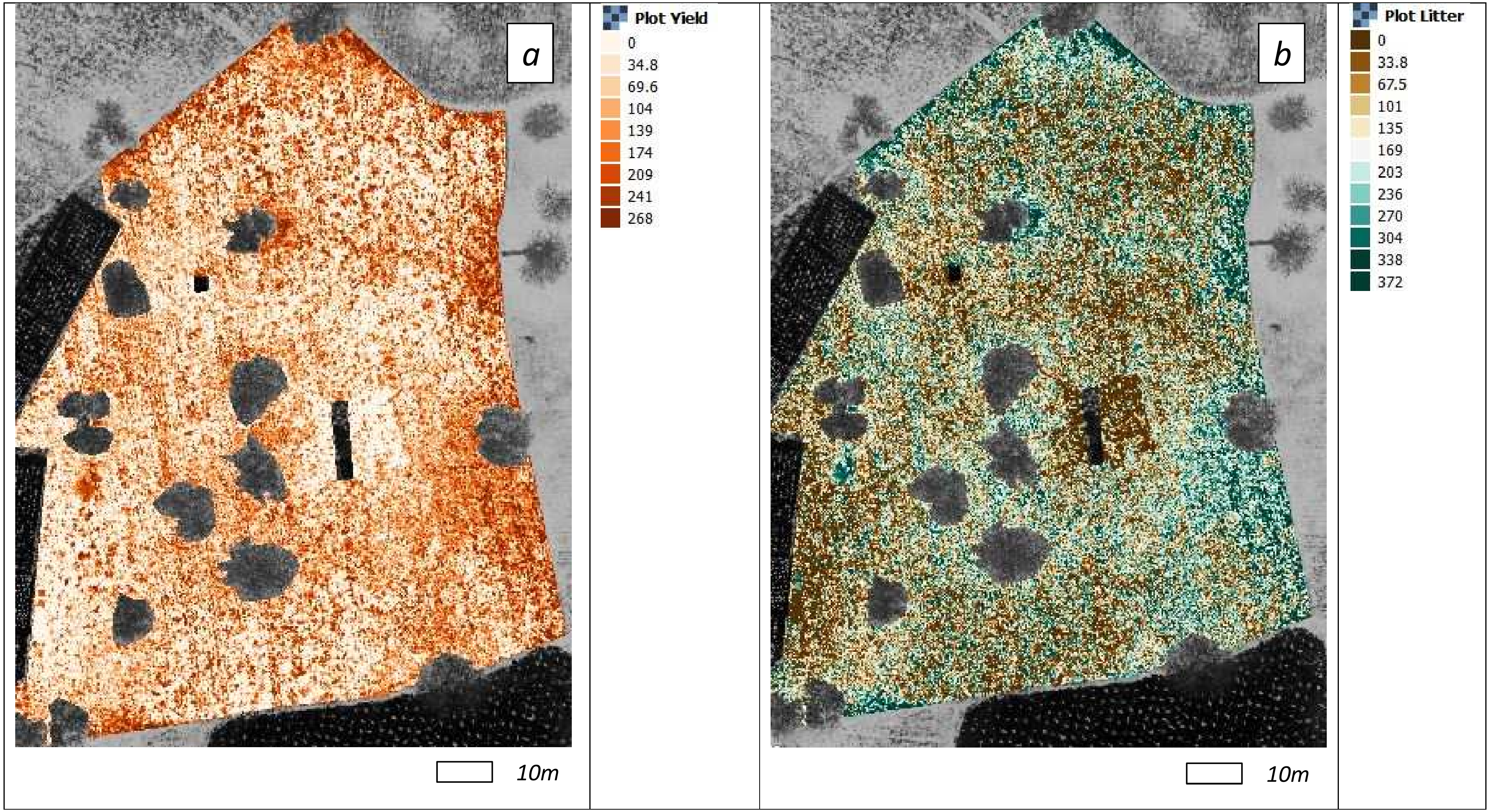

a
Plot Yield
0
34.8
69.6
104
139
174
209
241
268
10m
b
Plot Litter
0
33.8
67.5
101
135
169
203
236
270
304
338
372
10m

Table 1: One-way ANOVA statistics for effect of the *Faidherbia albida* tree upon average ± SD crop traits, as assessed in 12 harvest subplots according to three distances from the tree: below the tree crown (0.5 R), at 2.5 radii (2.5 R), and at 5 radii (5R), where R is the radius of the tree crown. N = 4 replicates (4 transects) per distance to tree.

Variable	0.5R	2.5R	5R	Variances homogeneity (Bartlett)	Normality of the residues (Shapiro)	Test	F-value	p-value
Grain Dry Mass (g_{grain} m^{-2})	a 135.60 ± 35.47	ab 76.49 ± 45.74	b 47.77 ± 32.89	0.85	0.14	ANOVA	5.43	0.028
Stem Dry Mass (g m^{-2})	a 156.06 ± 37.69	ab 86.61 ± 45.42	b 70.56 ± 31.86	0.85	0.42	ANOVA	5.51	0.027
Whole-plant Dry Mass (g m^{-2})	a 453.89 ± 118.12	ab 270.68 ± 135.27	b 209.94 ± 101.08	0.90	0.10	ANOVA	4.56	0.043
Weeds aerial Dry Mass (g m^{-2})	a 210.12 ± 53.48	ab 403.47 ± 76.28	b 689.20 ± 439.40	0.003	0.01	Kruskal-Wallis	-	0.021
Millet + Weeds Litter (gC m^{-2})	a 198.50 ± 52.10	ab 121.35 ± 53.80	a 99.47 ± 41.45	0.91	0.08	ANOVA	4.43	0.046
NDVI	a 0.54 ± 0.08	a 0.45 ± 0.03	a 0.47 ± 0.03	0.16	0.32	ANOVA	3.13	0.093
MSAVI2	a 0.63 ± 0.07	a 0.55 ± 0.03	a 0.56 ± 0.03	0.18	0.37	ANOVA	3.69	0.068
Leaf Dry Mass (g m^{-2})	a 59.76 ± 19.45	a 40.84 ± 14.95	a 33.45 ± 12.50	0.77	0.37	ANOVA	2.91	0.106
SLA (m_{leaf}^{-2} kg_{DM}^{-1})	a 10.37 ± 2.10	a 10.92 ± 1.60	a 10.97 ± 0.61	0.20	0.78	ANOVA	0.18	0.835
LAI (m_{leaf}^{-2} m_{soil}^{-2})	a 0.63 ± 0.28	a 0.44 ± 0.13	a 0.37 ± 0.15	0.39	0.99	ANOVA	1.96	0.197
Root Dry Mass (g m^{-2})	a 56.21 ± 21.05	a 32.07 ± 14.21	a 31.59 ± 17.45	0.82	0.15	ANOVA	2.51	0.136
Root-to-tot. ratio (g_{root} $g_{plant-1}$)	a 0.17 ± 0.03	a 0.19 ± 0.05	a 0.24 ± 0.09	0.25	1.00	ANOVA	1.26	0.330
Head minor effect (% or ear)	a 6.74 ± 4.60	a 7.59 ± 6.70	a 6.54 ± 3.36	0.54	0.48	ANOVA	0.05	0.953

Table 2: Correlation statistics between crop traits, or between NDVI or MSAVI2 and some crop traits, within the 12 harvested subplots.

Figure	Y Variable	X Variable	Equation	Normality of the residues (Shapiro)	r^2	RMSE	RRMSE (%)	p-value
7a	Millet grain yield ($g\ m^{-2}$)	Millet LAI ($m_{leaf}^2\ m_{soil}^{-2}$)	Y =194.347*X - 6.178	0.22	0.63	32.87	37.9	0.002
7b	Millet total dry mass ($g\ m^{-2}$)	Millet LAI ($m_{leaf}^2\ m_{soil}^{-2}$)	Y = 645.968*X + 3.055	0.23	0.80	71.84	23.1	<0.001
7c	LAI of millet + weeds ($m_{leaf}^2\ m_{soil}^{-2}$)	NDVI of millet + weeds	Y = 2.2956*X - 0.4054	0.79	0.47	0.15	21.6	0.014
7d	Millet grain yield ($g\ m^{-2}$)	NDVI of millet + weeds	Y = 551.1*X - 181.8	0.52	0.41	41.45	47.9	0.024
7e	Millet grain yield ($g\ m^{-2}$)	MSAVI2 of millet + weeds	Y = 594.3*X - 257.8	0.58	0.47	39.37	45.5	0.014
7f	Millet+weeds litter ($gC\ m^{-2}$)	NDVI of millet + weeds	Y = 706.2*X - 204.2	0.15	0.46	48.65	34.8	0.016

Table 3: Computation of pearl-millet yield and crop-partial Land Equivalent Ratio (LER_{cp}) from subplots to the whole-plot scale; comparison (error) between measurements (in subplots and at the whole-plot scale) and estimations via UAV-NDVI product. *Yi* is the yield in agroforestry used to compute LER_{cp}.

	Method	Variable of interest	Value	Unit
Whole-plot characteristics	QGIS	Whole plot area	8994	m^2
	QGIS	Shelter area	62	m^2
	QGIS	Trunk basal area	2.4	m^2
	QGIS	Whole plot effective area	8929	m^2
	Manual	Subplots area	226	m^2
	QGIS	*F. albida* canopy projected area	862	m^2
	QGIS	*F albida* canopy cover	9.6	%
Harvest	Measured	Subplots harvest	17.6	kgDM grain
	Measured	Whole-plot bundle harvest (without subplots)	52.0	# bundles
	Measured	Whole-plot bundle harvest (without subplots)	1214.6	kgDM bundles
	Measured	Rate of conversion bundle-to-grain	0.52	/
	Measured	Whole-plot grain harvest (without subplots)	632.0	kgDM grain
	Measured	Whole-plot harvest	650	kgDM grain
	UAV-NDVI (Estimated)	Estimated Whole-plot harvest	811	kgDM grain
Yield	Measured	Millet yield as sole crop (5R)	0.48	tDM grain ha-1
	Measured	Millet yield half-distance (2.5R)	0.76	tDM grain ha^{-1}
	Measured	Millet yield under tree crown (0.5R)	1.36	tDM grain ha^{-1}
	Measured	Whole-plot Yield	0.73	tDM grain ha^{-1}
	UAV-NDVI (Estimated)	Estimated Millet yield sole crop (dist>Range)	0.82	tDM grain ha-1
	UAV-NDVI (Estimated)	Estimated Millet yield agroforestry (Crown<dist<Range)	0.92	tDM grain ha-1
	UAV-NDVI (Estimated)	Estimated Millet yield agroforestry (dist<Crown)	1.21	tDM grain ha-1
	UAV-NDVI (Estimated)	Estimated Whole-plot Yield	0.91	tDM grain ha-1
	Error	Yield Error	19.9	%
LER_{cp}	UAV-NDVI (Estimated)	LER_{cp} with *Yi* = actual whole plot yield	1.10	/
	UAV-NDVI (Estimated)	LER_{cp} with *Yi* = whole plot yield for dist <Range	1.16	/
Millet+Weeds litter	UAV-NDVI (Estimated)	Estimated Litter (Crop + weeds)	1.05	tC ha-1